



# REPORT DOCUMENTATION PAGE

*Form Approved*  
OMB No. 0704-0188

Public reporting burden for this collection of information is estimated to average 1 hour per response, including the time for reviewing instructions, searching existing data sources, gathering and maintaining the data needed, and completing and reviewing this collection of information. Send comments regarding this burden estimate or any other aspect of this collection of information, including suggestions for reducing this burden to Department of Defense, Washington Headquarters Services, Directorate for Information Operations and Reports (0704-0188), 1215 Jefferson Davis Highway, Suite 1204, Arlington, VA 22202-4302. Respondents should be aware that notwithstanding any other provision of law, no person shall be subject to any penalty for failing to comply with a collection of information if it does not display a currently valid OMB control number. **PLEASE DO NOT RETURN YOUR FORM TO THE ABOVE ADDRESS.**

<b>1. REPORT DATE (DD-MM-YYYY)</b> 01-07-2011		<b>2. REPORT TYPE</b> Annual Summary		<b>3. DATES COVERED (From - To)</b> 1 JUL 2008 - 30 JUN 2011	
<b>4. TITLE AND SUBTITLE</b> Epigenetic Control of Prolyl and Asparaginyl Hydroxylases in Prostate Cancer				<b>5a. CONTRACT NUMBER</b>	
				<b>5b. GRANT NUMBER</b> W81XWH-08-1-0112	
				<b>5c. PROGRAM ELEMENT NUMBER</b>	
<b>6. AUTHOR(S)</b> Adam Case  E-Mail: adam-case@uiowa.edu				<b>5d. PROJECT NUMBER</b>	
				<b>5e. TASK NUMBER</b>	
				<b>5f. WORK UNIT NUMBER</b>	
<b>7. PERFORMING ORGANIZATION NAME(S) AND ADDRESS(ES)</b> University of Iowa Iowa City, IA 52242				<b>8. PERFORMING ORGANIZATION REPORT NUMBER</b>	
<b>9. SPONSORING / MONITORING AGENCY NAME(S) AND ADDRESS(ES)</b> U.S. Army Medical Research and Materiel Command Fort Detrick, Maryland 21702-5012				<b>10. SPONSOR/MONITOR'S ACRONYM(S)</b>	
				<b>11. SPONSOR/MONITOR'S REPORT NUMBER(S)</b>	
<b>12. DISTRIBUTION / AVAILABILITY STATEMENT</b> Approved for Public Release; Distribution Unlimited					
<b>13. SUPPLEMENTARY NOTES</b>					
<b>14. ABSTRACT</b> In many solid tumors, including prostate cancer, hypoxia-inducible factors (HIF) are up-regulated compared to their normal tissue counterparts. These HIF molecules are transcription factors, and up-regulate metabolic and angiogenic proteins in the cancer. Recently, a set of proteins known as prolyl and asparaginyl hydroxylases (PHD and AHD respectively) have been shown to be essential in the regulation of HIF, and in some cancers have been transcriptionally and translationally silenced. We therefore proposed a study that focuses on the epigenetic control of these crucial enzymes. In this report, we present data demonstrating our first findings of PHD expression in prostate cancer cell lines as well as expanding our studies to relevant human samples. Furthermore, we begin to identify specific epigenetic mechanisms that may play a major role in the transcriptional and translational control of these enzymes. Last, we will explain our future direction of the project after the award period has expired.					
<b>15. SUBJECT TERMS</b> Hypoxia Inducible Factor, HIF, Prolyl Hydroxylase, PHD, Prostate Cancer					
<b>16. SECURITY CLASSIFICATION OF:</b>			<b>17. LIMITATION OF ABSTRACT</b>	<b>18. NUMBER OF PAGES</b>	<b>19a. NAME OF RESPONSIBLE PERSON</b>
<b>a. REPORT</b>	<b>b. ABSTRACT</b>	<b>c. THIS PAGE</b>			<b>19b. TELEPHONE NUMBER (include area code)</b>
U	U	U	UU	36	USAMRMC

## Table of Contents

	<u>Page</u>
Introduction.....	5
Body.....	5-7
Key Research Accomplishments.....	7
Reportable Outcomes.....	8
Conclusion.....	9
Appendices (Figures).....	10-14
 <b>Attached Manuscripts</b>	

## Introduction

In many solid tumors, including prostate cancer, hypoxia-inducible factors (HIF) are up-regulated compared to their normal tissue counterparts. These HIF molecules are transcription factors, and up-regulate metabolic and angiogenic proteins in the cancer. Recently, a set of proteins known as prolyl and asparaginyl hydroxylases (PHD and AHD respectively) have been shown to be essential in the regulation of HIF, and in some cancers have been transcriptionally and translationally silenced. We therefore proposed a study that focuses on the epigenetic control of these crucial enzymes. In this report, we present data demonstrating our first findings of PHD expression in prostate cancer cell lines as well as expanding our studies to relevant human samples. Furthermore, we begin to identify specific epigenetic mechanisms that may play a major role in the transcriptional and translational control of these enzymes. Last, we will explain our future direction of the project after the award period has expired.

## Body

In our previous reports, we had begun the initial characterization of the PHD's and AHD in an array of prostate and breast cancer cell lines. In contrast with our initial hypothesis, the expression levels of PHD1, PHD2, and AHD did not significantly differ amongst the cancer cell lines compared to normal controls. On the contrary, the mRNA and protein level of PHD3 was quite variable amongst the cell lines assayed. Due to this observation, our initial statement of work was changed to focus on this specific isozyme. We attempted to examine the role of epigenetic silencing of PHD3 in these cell lines, and found that DNA methylation appeared to be a key regulator of the expression level of this protein. Furthermore, it was found that PHD3 could be reactivated if given a potent DNA de-methylating agent (5-aza-dC) demonstrating a causal relationship to the methylation of the PHD3 promoter and gene silencing. Since the time of our last report, we have confirmed and extended these results in numerous cancer cell lines of prostate, breast, and melanoma origins (Figure 1). The epigenetic silencing of PHD3 was not limited to DNA methylation, as it was observed that global chromatin structure was also altered around the PHD3 promoter (data shown in previous report). While these results are novel and exciting, using only carcinoma cell lines leaves questions about clinical relevance of our findings. To

address this issue, we have finalized studies upon prostate tumor samples extracted from human patients. It was discovered that on average the clinical tumors demonstrate significantly lower levels of PHD3 mRNA than normal prostate tissue (Figure 2). Unfortunately, the limited quantity of tumor per sample we were able to acquire prevented our ability to confirm these results at the protein level. In contrast, DNA methylation analysis was performed on these tissues and demonstrated little to no methylation at the PHD3 promoter regardless of expression level of PHD3 (data not shown). Two possibilities exist to explain this finding: 1) The region within the PHD3 promoter that was analyzed is methylated in cancer cell lines but not clinical tumor samples, or 2) other epigenetic processes may be involved in the silencing of PHD3 *in vivo*. Both of these hypotheses provide enticing endeavors for the future of this project.

With the understanding that DNA specific epigenetic marks may not explain the entire story of control of PHD3, we attempted to examine other avenues of gene expression regulation. When examining the specific prostate cancer cell line DU145, it was observed that these cells had attenuated PHD3 expression that could be reversed by hypoxia but exhibited no methylation at the PHD3 promoter (see attached manuscript for full data). These data suggest another level of mRNA regulation beyond DNA methylation. Using the miRNA prediction software TargetScan, we were able to discover 4-5 potential miRNA binding sites in the PHD3 3' untranslated region (UTR) (Figure 3). These miRNA sites may play a major role in the regulation of PHD3 mRNA levels post-transcriptionally, and could be a novel regulatory element not yet described for this gene. To examine if these miRNA binding sites do play a role in the control of PHD3, we cloned the 3' UTR of PHD3 into a vector downstream of a luciferase gene. By doing this, we allowed the stability of luciferase to be controlled by the same regulator elements that may impact the stability of PHD3. Interestingly, when this vector was transfected into DU145 prostate cell lines it was observed that the stability of luciferase was decreased almost 50%, and hypoxia demonstrated no significant change in this reduction (Figure 4). While these data are preliminary, they are highly suggestive of expression regulatory regions within the 3' UTR of PHD3. Future work on this project will attempt to elucidate the exact mechanism by which PHD3 is controlled post-transcriptionally; a new aspect of this project not fully appreciated at the start.

Finally, a very recent discovery has shed new light on the functional role of PHD3. Luo *et al.* (Cell. 2011 May 27;145(5):732-44.) have shown that PHD3 may interact with and disrupt the function of pyruvate kinase in a hydroxylase independent manner. This finding implies that PHD3 may have a direct impact on cellular metabolism, as opposed to an indirect effect through the hypoxia inducible factors (HIFs). To query if this indeed was true, we examined if the presence of PHD3 could change the amount of oxidative stress (an indirect measure of metabolism) within cancer cells. Using an adenovirus to over-express PHD3, we infected the pancreatic cell line Mia-PaCa2 (this cell line was used due to its high infectivity with adenovirus, as well as undetectable expression of endogenous PHD3). It was observed that the over-expression of PHD3 in these cell lines decreased dihydroethidium oxidation by approximately half, suggesting a 50% reduction in cellular reactive oxygen species (Figure 5). These data support a direct metabolic alteration by the presence of PHD3, and warrants further investigation into the exact mechanism of how this may affect tumor cell growth and proliferation.

In summary, we have thoroughly characterized the epigenetic processes of DNA methylation and chromatin structure at the PHD3 promoter as initially outlined in our statement of work. While certain avenues of this project did not produce the anticipated results, the project produced significant findings in the regulation of PHD3. It is our goal to continue elucidating novel mechanisms of control of this enzyme in the hopes of potential new therapies for patients with prostate cancer.

### **Key Research Accomplishments**

- Completion of PHD3 expression analysis on clinical tumor samples
- Completion of PHD3 promoter methylation analysis on clinical tumor samples
- Identification of putative microRNA binding sites, and preliminary regulatory studies using the 3'UTR of PHD3 on a luciferase reporter
- Oxidative stress analysis on prostate carcinoma cell line in the presence and absence of PHD3, with the potential for understanding metabolic changes due to PHD3

## Reportable Outcomes

### Peer-reviewed publications:

- Place TL, Fitzgerald MP, Venkataraman S, **Case AJ**, Vorrink S, Teoh MLT, Domann FE. *Aberrant Promoter CpG Methylation Is a Mechanism for Impaired PHD3 Expression in a Diverse Set of Malignant Cells*. PLoS One. 2011 Jan 28;6(1):e14617.
- **Case AJ**, McGill JL, Tygrett LT, Shirasawa T, Spitz DR, Waldschmidt TJ, Legge KL, Domann FE. *Elevated mitochondrial superoxide disrupts normal T cell development, impairing adaptive immune responses to an influenza challenge*. Free Radic Biol Med. 2011 Feb 1;50(3):448-58.
- **Case, A.J.** et al (2011). *The conditional loss of SOD2 results in an erythropoietic protoporphyria-like phenotype*. (In preparation for JBC).

### Abstracts:

- **Case AJ**, and Domann FE. *A Novel Role for Mitochondrial Superoxide in the Development of Erythropoietic Protoporphyria*. Free Radical Biology and Medicine. 49 (1): S92.
- **Case AJ**, Place TL, Fitzgerald MP, Venkataraman S, Vorrink S, Teoh, MLT, Bera S, Goel A, Domann FE. *Aberrant Promoter CpG Methylation Is a Mechanism for Impaired PHD3 Expression in a Diverse Set of Malignant Cells*. IMPaCT Conference (2011).
- Cyr AR, **Case AJ**, Mao GW, Domann FE. *Conditional Knockout of Sod2 in Murine Hepatocytes Disrupts Epigenetic Control of Gene Expression*. Free Radical Biology and Medicine. 49 (1): S128.
- Mao GW, Jacobus JA, Martin SM, **Case AJ**, Aykin-Burns N, Mapuskar K, Coleman MC, Gius D, Domann FE, Spitz DR. *Low Dose (10-100 cGy) Whole Body Irradiation Increases Steady-state Levels of Superoxide in C57BL/6 Thymocytes*. Free Radical Biology and Medicine. 49 (1): S66

### Awards/Degrees:

- **Case AJ**. - PhD in Free radical and radiation biology – May, 2011
- **Case AJ**. – Travel Award – Society for Free Radical Biology and Medicine annual conference – November 2010

## **Conclusion**

In summary, this project has surpassed its initial goals as outlined prior to the funding period. Initially, our study was limited to basic expression and DNA methylation analysis, but we have expanded our abilities to include genetic manipulations, in-depth oxygen tension studies, miRNA studies, as well as metabolic examinations. This work has produced a peer-reviewed journal article in a highly regarded journal, and others are in preparation. We hope to continue our findings on PHD3 in the future, and anticipate new students to take on the challenges of elucidating even more novel findings with this enzyme.

The PI of this work has achieved numerous other manuscripts, research awards, and has presented his work at a variety of national conferences around the United States. Furthermore, as of May, 2011 and the end of the award period, the PI successfully completed his PhD studies and is pursuing a 1-year transition post-doctoral fellowship with Dr. Domann prior to pursuing his career in medicine/research.

Appendices – Figure 1

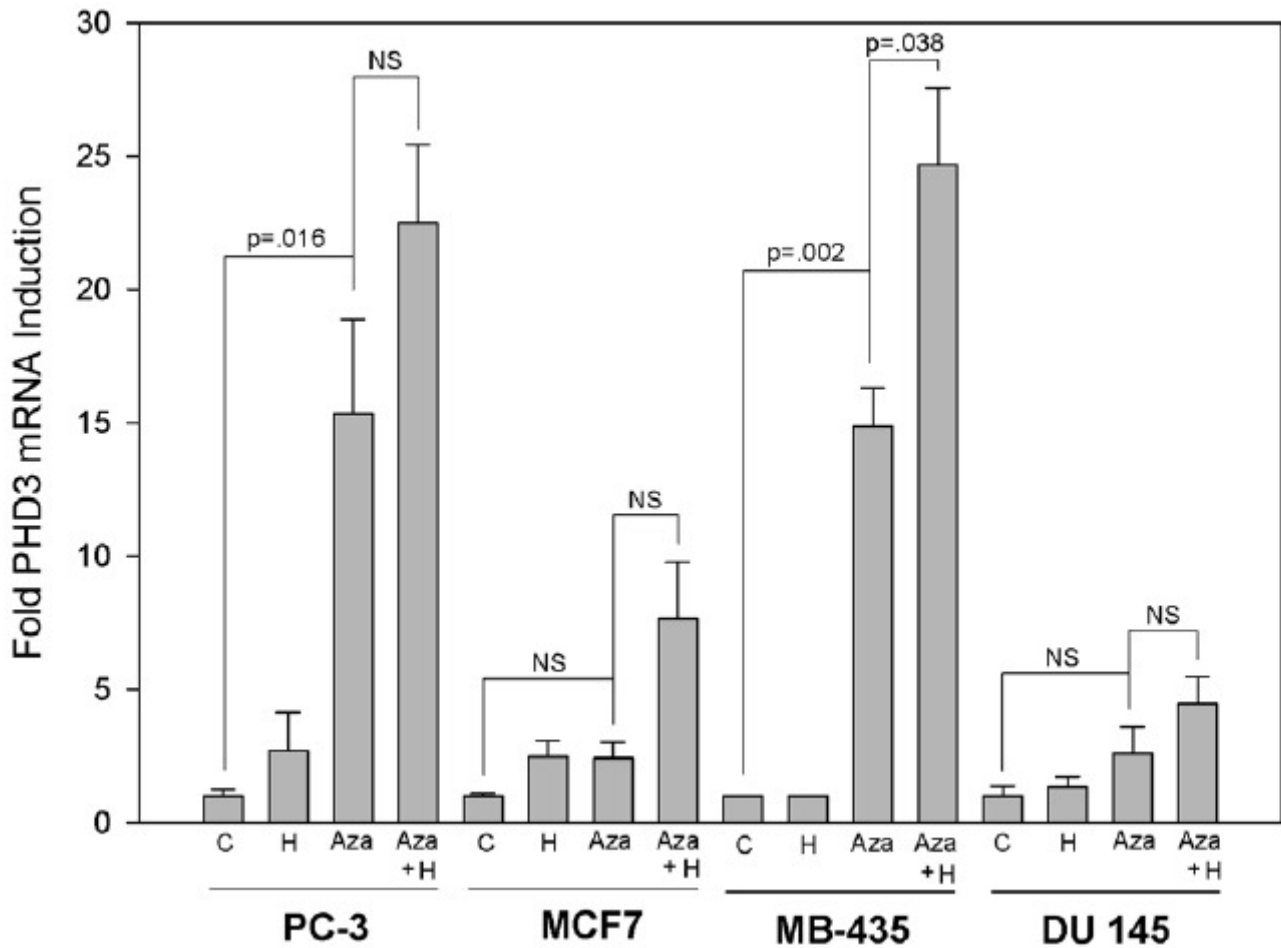


**Figure 1.** Cell lines representative of PHD3 expressers and PHD3 non-expressers were either not treated (C), treated with hypoxia (H), treated with 5-Aza-dC (Aza), or treated with 5-Aza-dC and then subjected to 1% oxygen (Aza + H). Real time quantitative PCR was performed to determine the mRNA expression of PHD3. The data were normalized to GAPDH and expressed relative to PHD3 mRNA in the corresponding untreated controls. Error bars = SEM. n = 3.

## Appendices – Figure 2

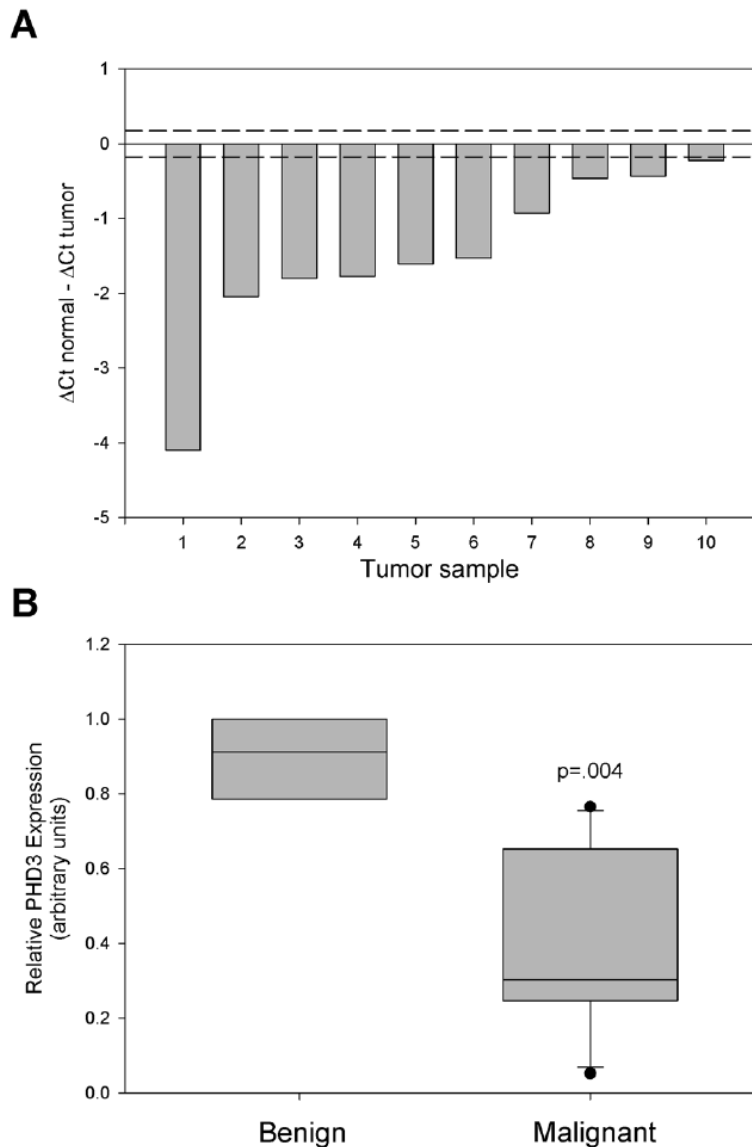


**Figure 2.** PHD3 mRNA expression is down-regulated in multiple primary human prostate cancer specimens. A) Total mRNA was isolated from frozen sections of primary human prostate cancer specimens with Gleason scores ranging from 7–9. Quantitative real-time PCR was performed using PHD3 specific TaqMan primer-probe. Relative PHD3 mRNA expression for each tumor sample is represented as (average dCt of  $n = 3$  benign prostate tissue samples) – (dCt tumor sample). Samples were normalized to GAPDH. Dotted lines represent  $\pm 2$  1 SD for benign tissue PHD3 mRNA expression. B) Box plot depicting PHD3 mRNA expression from samples shown in A. p value is based on ANOVA between 3 benign samples and 10 malignant samples.



Human EGLN3 3' UTR

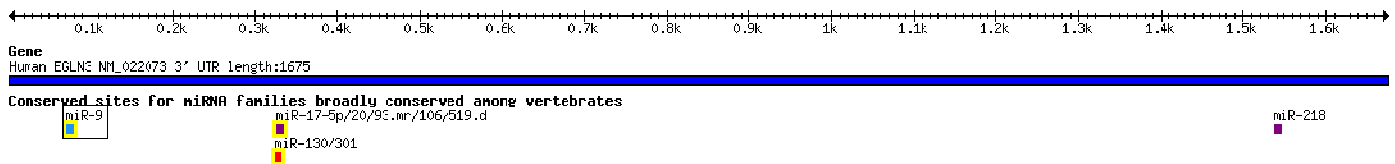


**Figure 3.** TargetScan analysis of 3'UTR of PHD3. When analyzing the untranslated region of PHD3 four major putative microRNA binding sites are elucidated.

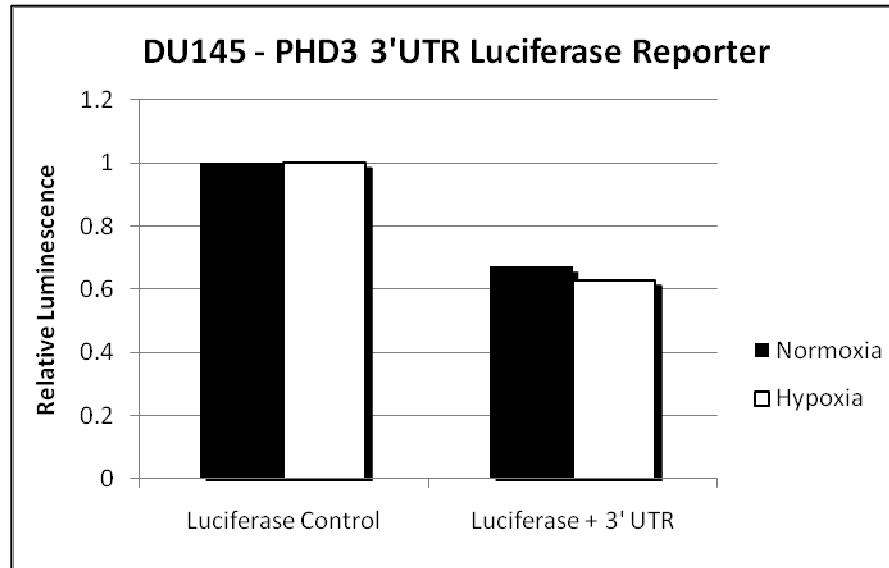


**Figure 4.** The 3' UTR of PHD3 destabilizes the reporter gene luciferase. After successfully cloning the 3' UTR of PHD3, the segment of DNA was placed downstream of a luciferase construct. When transfected into DU145 cells, it was discovered that the placing luciferase under the regulatory control of the 3' UTR demonstrated an approximate 50% decrease in luciferase stability.

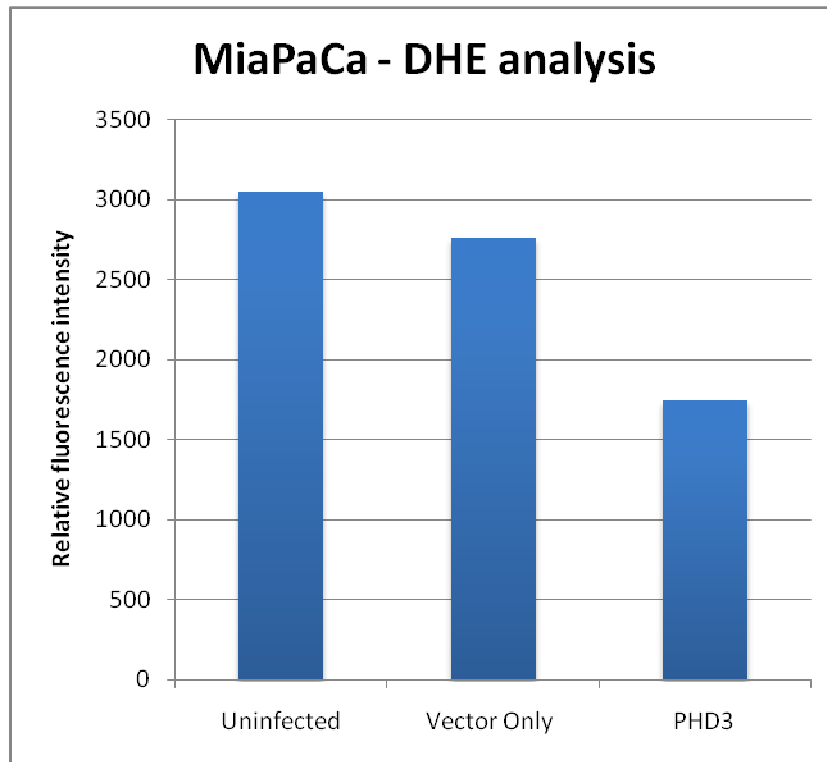


**Figure 5.** The over-expression of PHD3 reduces cellular reactive oxygen species. Mia-PaCa2 cells were transfected with a mammalian expression vector of PHD3, and then exposed to dihydroethidium as a direct measure of cellular reactive oxygen species. The presence of PHD3 reduced dihydroethidium staining by approximately 50%.

# Aberrant Promoter CpG Methylation Is a Mechanism for Impaired PHD3 Expression in a Diverse Set of Malignant Cells

Trenton L. Place<sup>1</sup>\*, Matthew P. Fitzgerald<sup>2</sup>\*, Sujatha Venkataraman<sup>3</sup>\*, Sabine U. Vorrink<sup>4</sup>, Adam J. Case<sup>2</sup>, Melissa L. T. Teoh<sup>2</sup>, Frederick E. Domann<sup>1,2,4,5</sup>\*

**1** Molecular and Cellular Biology Program, The University of Iowa, Iowa City, Iowa, United States of America, **2** Free Radical and Radiation Biology Program and Department of Radiation Oncology, The University of Iowa, Iowa City, Iowa, United States of America, **3** University of Colorado Denver, Pediatrics, Aurora, Colorado, United States of America, **4** Human Toxicology Program, The University of Iowa, Iowa City, Iowa, United States of America, **5** Carver College of Medicine and The Holden Comprehensive Cancer Center, The University of Iowa, Iowa City, Iowa, United States of America

## Abstract

**Background:** The prolyl-hydroxylase domain family of enzymes (PHD1-3) plays an important role in the cellular response to hypoxia by negatively regulating HIF- $\alpha$  proteins. Disruption of this process can lead to up-regulation of factors that promote tumorigenesis. We observed decreased basal expression of PHD3 in prostate cancer tissue and tumor cell lines representing diverse tissues of origin. Furthermore, some cancer lines displayed a failure of PHD3 mRNA induction when introduced to a hypoxic environment. This study explores the mechanism by which malignancies neither basally express PHD3 nor induce PHD3 under hypoxic conditions.

**Methodology/Principal Findings:** Using bisulfite sequencing and methylated DNA enrichment procedures, we identified human PHD3 promoter hypermethylation in prostate, breast, melanoma and renal carcinoma cell lines. In contrast, non-transformed human prostate and breast epithelial cell lines contained PHD3 CpG islands that were unmethylated and responded normally to hypoxia by upregulating PHD3 mRNA. Only treatment of cells lines containing PHD3 promoter hypermethylation with the demethylating drug 5-aza-2'-deoxycytidine significantly increased the expression of PHD3.

**Conclusions/Significance:** We conclude that expression of PHD3 is silenced by aberrant CpG methylation of the PHD3 promoter in a subset of human carcinoma cell lines of diverse origin and that this aberrant cytosine methylation status is the mechanism by which these cancer cell lines fail to upregulate PHD3 mRNA. We further show that a loss of PHD3 expression does not correlate with an increase in HIF-1 $\alpha$  protein levels or an increase in the transcriptional activity of HIF, suggesting that loss of PHD3 may convey a selective advantage in some cancers by affecting pathway(s) other than HIF.

**Citation:** Place TL, Fitzgerald MP, Venkataraman S, Vorrink SU, Case AJ, et al. (2011) Aberrant Promoter CpG Methylation Is a Mechanism for Impaired PHD3 Expression in a Diverse Set of Malignant Cells. PLoS ONE 6(1): e14617. doi:10.1371/journal.pone.0014617

**Editor:** Joy Sturtevant, Louisiana State University, United States of America

**Received:** April 12, 2010; **Accepted:** January 3, 2011; **Published:** January 28, 2011

**Copyright:** © 2011 Place et al. This is an open-access article distributed under the terms of the Creative Commons Attribution License, which permits unrestricted use, distribution, and reproduction in any medium, provided the original author and source are credited.

**Funding:** This work was supported by National Institutes of Health (NIH) grants R01CA115438 (FED), R01CA073612 (FED), DOD grant W81XWH-08-1-0112 (AJC), and the Susan G. Komen for the Cure grant KG080437 (MLT). SV received a project development grant from NIH Cancer Center Support, grant P30CA086862. SUV received partial salary support from NIEHS 2P42ES013661, and AJC received partial salary support from NIH T32GM073610. The funders had no role in study design, data collection and analysis, decision to publish, or preparation of the manuscript.

**Competing Interests:** The authors have declared that no competing interests exist.

\* E-mail: frederick-domann@uiowa.edu

† These authors contributed equally to this work.

‡ Current address: Department of Pediatrics – Peds Hem-Onc, University of Denver, Denver, Colorado, United States of America

## Introduction

The cellular response to reduced oxygen availability (hypoxia) is controlled by a class of proteins called hypoxia-inducible factors (HIF- $\alpha$ ). There are 3 known isoforms of HIF-1 $\alpha$ : HIF-1 $\alpha$ , HIF-2 $\alpha$  and HIF-3 $\alpha$ . HIF-1 $\alpha$  and HIF-2 $\alpha$  are transcription factors. HIF-3 $\alpha$  appears to lack transcriptional activity and may play a role in negative regulation of the HIF pathway [1]. Thus, from here on, when referring to HIF- $\alpha$ , we are referring to only HIF1 and HIF2. Transcriptionally active HIF1 and 2 are heterodimers composed of the HIF- $\alpha$  subunit and aryl hydrocarbon nuclear translocator receptor (ARNT/HIF- $\beta$ ). HIF-1 $\alpha$  activates the transcription of EPO, VEGF, heme oxygenase-1 and several other critical

intracellular responses to hypoxia including enzymes of the glycolytic pathway [2,3]. While less is known about HIF-2 $\alpha$  transcriptional targets, HIF-2 $\alpha$  appears to play a lesser role in the glycolytic response with more emphasis on EPO and VEGF transcription [4].

HIF- $\alpha$  mRNA levels are generally stable in cells. It is not until after translation that HIF- $\alpha$  is tightly controlled. During periods of normal physiological oxygen concentration, HIF- $\alpha$  subunits are kept at low levels by constant proteolytic degradation. First, a hydroxylation reaction is catalyzed by a family of prolyl hydroxylase domain-containing proteins (PHD/EGLN/HPH) which utilize iron, oxygen and 2-oxoglutarate as co-factors to enzymatically catalyze hydroxylation on the oxygen-dependent

degradation domain (ODD) of the HIF $\alpha$  -subunit [5]. Hydroxylated proline residues on HIF- $\alpha$  are recognized by Von Hippel-Lindau (VHL) protein, an E3 ubiquitin ligase that ubiquitinates the HIF- $\alpha$  subunit, targeting it to the proteasome [6]. Under hypoxic conditions, HIF prolyl hydroxylase activity is decreased and HIF-1 $\alpha$  protein accumulates. HIF- $\alpha$  subunits translocate to the nucleus and dimerize with the constitutively expressed ARNT subunit [7,8]. This heterodimer acts to turn on transcription of genes involved in oxygen homeostasis and glucose metabolism [2].

Three main isoforms of HIF prolyl-hydroxylase domain containing proteins, PHD1-3, have been identified [9]. These isoforms have been reported to have different specificities for HIF-1 $\alpha$  and HIF-2 $\alpha$  [10], and also differ in their subcellular localization. It has been shown that PHD1 is exclusively present in cytoplasm, PHD2 is mainly located in the nucleus and PHD3 is evenly distributed in both cytoplasm and nucleus [11]. PHD2 and PHD3, however, are considered to be the major isoforms that contribute to HIF-1 and -2 $\alpha$  degradation in cells [12,13]. In normoxia, PHD2 is the primary enzyme that hydroxylates HIF-1 $\alpha$  [14], whereas PHD3 has been reported to play an important role in HIF-2 $\alpha$  hydroxylation and also in retaining cellular hydroxylation capacity in a hypoxic environment [10,15].

In normal cells, PHD3 mRNA and protein are expressed at low levels during normoxia, but are significantly induced upon exposure to hypoxia. In contrast, PHD3 expression in a significant number of cancer cell types has been shown to be low or absent not only during normoxia, but also under hypoxic conditions [10,16]. To date, no mechanism has been discovered to explain this defect in hypoxic inducibility. Interestingly, Hatzimichael et al. have recently demonstrated that the promoter of PHD3 is methylated in certain primary B-cell dyscrasias [17]. We had observed a decrease in PHD3 mRNA expression in human breast and prostate carcinoma cell lines, with an absence of PHD3 upregulation in response to hypoxia. Therefore, we were interested to determine whether PHD3 promoter methylation was responsible for this aberrant expression pattern. In this study, we show that the promoter region of PHD3 is methylated in representative human prostate carcinoma, melanoma, renal carcinoma and breast cancer cell lines. Furthermore, we show that neither HIF-1 $\alpha$  protein levels nor hypoxic response through an HRE-luciferase reporter vector are compromised in PHD3 methylated compared to non-methylated cell lines. These results indicate that PHD3 promoter methylation is utilized by malignancies derived from diverse human cell types. Furthermore, these data suggest that loss of PHD3 expression may not affect the transcriptional response through the HIF pathway, leaving open the possibility that PHD3 silencing in tumors is selected through the loss of specific interactions with other cellular pathways.

## Methods

### Cell culture

Normal human prostate epithelial cells (NPREc) were purchased from Clonetics, Lonza Inc. (Walkersville, MD) and were grown on the recommended PrEGM media supplied by Clonetics, Lonza Inc. The hTERT-HME1 cells were cultured in mammary epithelial basal medium MEGM (Lonza Inc.) at 37°C and 5% CO<sub>2</sub> according to the manufacturer's instructions (Lonza Inc.). The DU 145, 22RV.1, PC-3, MDA-MB-435 (MB-435), and MCF7 cell lines were obtained from ATCC (Manassas, VA). MCF7, DU145 and MDA-MB-435 cells were cultured in Eagle's Minimum Essential Medium (MEM) supplemented with 10% fetal bovine serum (FBS). PC-3 cells were cultured in F12 medium supplemented with 10% FBS, 2 mM L-glutamine, 1 mM Na

Pyruvate, and supplemented with 100 U/ml pen/strep. All cell lines were routinely maintained at 37°C in a humidified atmosphere with 5% CO<sub>2</sub>. Fresh media was replaced every three days while routine subculture was performed by washing with 1X PBS and detaching cells with TrypLE Express.

### Semi-quantitative RT-PCR

Total RNA was extracted from individual cell lines using RNeasy Mini Kit (Qiagen, Valencia, CA) and quantified using a NanoDrop 1000. To assess *PHD3* and GAPDH expression, 500 ng of total RNA was used for reverse transcription using a OneStep RT-PCR Kit (Qiagen). The *PHD3* forward primer is 5'-GGGCAAATAC-TACGTCAAGGAG-3' and the reverse primer is 5'-AGTCTT-CAGTGAGGGCAGATTC-3'. GAPDH expression was assessed using GAPDH-specific primers. PCR conditions for *PHD3* and GAPDH were the same except that 28 cycles of PCR were performed for *PHD3* analysis and 23 cycles were performed for GAPDH. The parameters used were: 95°C for 5 minutes followed by the stated number of cycles of 94°C for 1 minute; 56°C for 1 minute, and 72°C for 1 minute, ending with a final extension at 72°C for 7 minutes. The amplified products were electrophoresed on a 1% agarose gel and stained with ethidium bromide to visualize the bands.

### Quantitative real time RT-PCR

Total RNA was isolated from cells using Trizol, followed by DNase treatment and NaOAc precipitation. The reverse transcription reaction was carried out with High-Capacity cDNA Archive Kit (Applied Biosystems, Foster City, CA). PHD3 TaqMan primer-probe was utilized from Applied Biosystems (Hs00222966\_m1). The quantitative real-time PCR was set up as follows: 10 ng of RNA was used as template for each real-time PCR reaction (10  $\mu$ g reaction volume); primer pairs at 0.3  $\mu$ M for GAPDH with Syber Green Master Mix (Applied Biosystems). For PHD3, TaqMan universal master mix was used. The DNA polymerase was activated by heat at 95°C for 10 min followed by 40 cycles, denaturing at 95°C for 15 s, annealing and elongating at 60°C for 1 min. Data were collected with ABI PRISM 7000 sequence detection system. Data were analyzed using the  $\Delta\Delta$ Ct method.

### Western Blot analysis

Cells were immediately washed with ice cold phosphate-buffered saline (pH 7.4). Cells were lysed on the plate in 200  $\mu$ l RIPA cell-lysis buffer (50 mM Tris pH 8.0, 150 mM NaCl, 0.1% SDS, 0.5% Na Deoxycholate, 1% TX-100) plus 1 mM NaF, 10 mM NaVO<sub>4</sub>, 10 mM PMSF, and 1/100 protease inhibitor cocktail (Sigma), immediately boiled for 2 minutes and then sonicated. SDS-polyacrylamide gels (7%, PHD3; 15% HIF1, HIF2) were used for protein electrophoresis. Proteins were electrotransferred onto nitrocellulose membranes and treated with anti HIF-1 $\alpha$  (Abcam, Cambridge, MA) 1:500 overnight at 4°C. Anti PHD3, NB100-139 and anti HIF-2 $\alpha$  antibodies (Novus Biologicals, Littleton, CO) were used at 1:500 and 1:200 respectively overnight at 4°C. Equal protein loading was confirmed on all immunoblots using human actin antibody (Sigma, St. Louis, MO) at a dilution 1:2000. Goat anti-rabbit IgG (BD Transduction Laboratories, San Diego, CA) was used as a secondary antibody against all primary antibodies. Bands were visualized by chemiluminescence with ECL plus reagent (Pierce, Rockford, IL) on a Typhoon FLA 7000.

### Sodium bisulfite sequencing

Genomic DNA was extracted with the use of the DNeasy Tissue Kit (Qiagen, Valencia, CA), and sodium bisulfite conversion was

performed with the use of the EZ DNA Methylation Kit (Zymo Research Corporation, Orange, CA). A pair of primers was designed to amplify the PHD3 promoter of both bisulfite modified methylated and unmethylated DNA but not unmodified DNA. Nested PCR amplification on converted DNA used the following primers: outside forward: 5'-GTGTGGGATTTAGGTTTT-TAAG-3' (SB1); outside reverse: 5'-CCAAATCCAACCTCA-TAATATATC-3' (SB2); and nested inner primers (SB3) and (SB4) whose sequences and locations are described in detail below.

The resulting PCR products were gel-extracted with the use of the Qiagen Gel Extraction Kit, or gel digestion with  $\beta$ -agarase followed by EtOH precipitation, and cloned with the TOPO TA Cloning Kit (Invitrogen). Plasmid DNA was extracted with the use of the QiaPrep Spin Plasmid Miniprep Kit (Qiagen). Sequencing was performed by the sequencing core facility maintained by the University of Iowa and results were tabulated for methylation status of each of the 58 CpGs contained in the amplicons from each cell line.

### 5-Aza-dC treatment

Cells were counted, and seeded (day 0) at approximately 750,000 cells/100 mm dish. Fresh 5-Aza-dC (5 mM) was added to the dish on days 1, 3, and 5 while a control flask was left untreated. On day 5, 5-Aza-dC treated cells were split into two 60 mm dishes in media supplemented with 5 mM 5-Aza-dC. On day 6, one of each of the 60 mm dishes was placed in a hypoxia chamber and placed under 1% O<sub>2</sub>, 94% N<sub>2</sub> and 5% CO<sub>2</sub> at 37°C. On day 7, all cells were harvested with 500  $\mu$ l Trizol for RNA extraction.

### Chromatin Accessibility

Chromatin accessibility experiments were conducted as previously described by Rose *et al.* [18]. The primers CA1 and CA2 were located within the region of the *PHD3* gene queried for DNA methylation (primer sequences and locations described in detail below). After nuclei extraction and a 5 minute DNase I digestion the DNA was extracted and real-time PCR was conducted on an ABI 7000 Sequence Detection System. The accessibility index for each amplicon was then determined by the following formula (accessibility index =  $2^{((\Delta Ct_{DNase\ treated}) - (\Delta Ct_{Uncut}))}$ ). GAPDH chromatin accessibility was also determined as a positive control for a constitutively expressed gene to control for equivalent DNase digestion between the cell lines examined.

### HRE-Luciferase assay

Cell lines ~85% confluent in 60 mm dishes were transfected with an HRE-luciferase reporter vector [19] (2.5  $\mu$ g) and Renilla luciferase (1.5  $\mu$ g) according to Lipofectamine 2000 transfection reagent protocol. Transfection media was removed after 6 hours and replaced with fresh medium. Cells were then placed under 94% N<sub>2</sub>, 5% CO<sub>2</sub>, 1% O<sub>2</sub> gas mixture in a hypoxia chamber, or normoxia for 24 hours and then lysed according to the Dual luciferase reporter assay system (Promega, Madison, WI) protocol. Luminescence was measured 3 times per sample using a Tecan SpectraFluor Plus luminometer.

### Adenoviral Transduction

The adenoviral PHD3 construct was a generous gift from Dr. Robert Freeman from Rochester University (unpublished). Briefly, the human PHD3 coding sequence was engineered into the pDC315 vector and contains an N-terminal FLAG tag. PC3 cells were grown to ~85% confluency and then transduced with 20, 40 or 60 MOI of Ad-PHD3. Approximately 36 hours following transduction, cells were lysed with

RIPA buffer and western blotted according to the procedures outlined above.

### Clinical Samples

Clinical prostate tumor samples were received as frozen blocks in OCT. Sections were cut and ground with mortar and pestle. DNA and RNA were extracted in with Qiagen DNeasy Tissue kit and Trizol respectively.

### Methylated DNA Enrichment

Genomic DNA was harvested from cells and tissue using a Qiagen DNeasy Tissue kit. 2  $\mu$ g of DNA in 120  $\mu$ l of 10 mM Tris pH 8.0 was sonicated into fragments of approximately 150 bp using a Covaris S2. Fragmentation was done according to the Covaris protocol. 1  $\mu$ g (60  $\mu$ l) of sheared input gDNA was used according to the protocol supplied by the MethylMiner kit (Invitrogen). Binding reactions between beads containing methyl-CpG binding domains and sheared genomic DNA were performed at 4°C overnight. Bound DNA was eluted using progressively increasing NaCl concentrations. Eluates were precipitated using NaOAc and EtOH precipitation and resuspended in 60  $\mu$ l 10 mM Tris pH 8.0. Real time PCR was performed using 1  $\mu$ l resuspended DNA, SYBR Green master mix and 100 nM Fwd Primer: 5'-GAGCTCCACGACCCGTTTC-3' and Rev Primer: -5'-GCAGTGGTGGCTTCCCAT-3' in a 10  $\mu$ l reaction volume. The kit was validated using samples from human tumor cell lines with known *PHD3* CpG island methylation status as determined by bisulfite sequencing (**Figure S1**).

### Statistical Analysis

Significant differences between groups of data were determined using a t-test for all bar graphs or ANOVA for box plot powered by SigmaPlot 11.0 software. n = 3 was used for each data set unless otherwise noted.

## Results

### PHD3 mRNA is aberrantly silenced in human melanoma, prostate and breast carcinoma cell lines

A panel of human carcinoma cell lines was screened for PHD3 mRNA expression. This panel consisted of three prostate cancer cell lines (DU 145, 22RV.1 and PC-3), two breast cancer cell lines (MCF7, HS578T), one melanoma (MDA-MB-435), a non-transformed prostate epithelial cell line (NPrEC) and a non-transformed, immortalized breast cell line (hTERT-HME1). We found that PHD3 mRNA was expressed at different levels varying from abundant to almost undetectable levels as determined by conventional RT-PCR (**Figure 1a**). The prostate cancer cell lines showed decreased PHD3 mRNA expression compared to the normal prostate epithelial cells. A comparison of three prostate cancer cell lines showed that PHD3 is expressed in DU 145 and 22 RV.1, whereas in PC-3, PHD3 mRNA is nearly undetectable. The melanoma cell line, MDA-MB-435 was also found to have very low PHD3 mRNA expression. Among the mammary cell lines, HS578T had much lower PHD3 mRNA than the HME1 mammary epithelial cells and MCF7 cells expressed far more PHD3 mRNA than its normal HME1 mammary epithelial cell counterpart. To confirm and extend the results shown in **Figure 1a**, quantitative real time RT-PCR analysis of PHD3 mRNA expression were conducted and the results are shown in **Figure 1b**. Similarities in expression were found with both the methods used, and PHD3 mRNA expression was nearly undetectable in PC-3, MDA-MB-435 and HS578T cell lines.

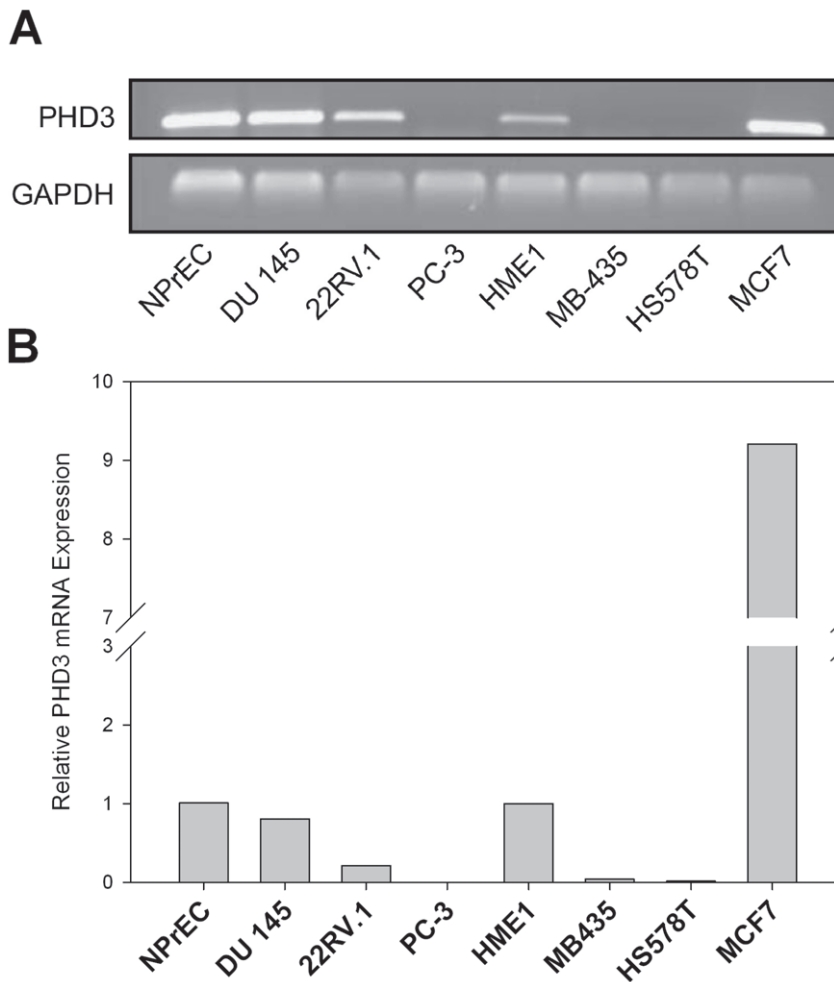


**Figure 1. Differential expression of PHD3 mRNA in normal and tumor cell lines of prostate, breast and melanoma origin.** Total RNA was extracted from the indicated cell lines. **A)** Expression of mRNA was determined by semiquantitative RT-PCR using specific primers designed to amplify PHD3 and GAPDH. The RT-PCR products were electrophoresed using 1% agarose gel, with ethidium bromide to show bands of expected sizes. GAPDH was used as the loading control. **B)** Quantitative real-time reverse transcription-PCR analysis of *PHD3* was performed with normalization to 18S rRNA gene expression and relative quantities were determined by the DDCT method. The data shown are the *PHD3* gene expression of individual cancer cell lines relative to those of their corresponding normal counterparts (PrEC for prostate and HMEC-hTERT for mammary). doi:10.1371/journal.pone.0014617.g001

### Re-expression of PHD3 with DNA methyltransferase inhibitor 5-Aza-dC

The near absence of PHD3 mRNA expression in a subset of cell lines suggested an epigenetic mechanism might be responsible for their silencing. Unlike genetic mutations that accumulate in cancer, epigenetic modifications are reversible [20]. We hypothesized that if DNA methylation of the *PHD3* gene was responsible for its reduced expression, a DNA methyltransferase inhibitor such as 5-Aza-2'-deoxycytidine (5-Aza-dC) should induce its expression. This is in line with 5-Aza-dC's purported ability to re-activate genes previously silenced by DNA methylation in cancer cells [21]. We chose 2 cell lines displaying the most marked decrease in PHD3 expression, MB-435 and PC-3, and 2 cell lines displaying moderate to high basal PHD3 expression, MCF7 and DU 145 for treatment with 5-Aza-dC. When MB-435 and PC-3 cells were treated with 5-Aza-dC, there were significant increases in the PHD3 mRNA expression compared to their respective untreated controls (**Figure 2**). Furthermore, MB-435 cells became responsive to PHD3 mRNA upregulation by hypoxia to a significant

degree following hypoxic exposure. Cells that already expressed PHD3 at moderate levels did not respond to 5-Aza-dC by significantly upregulating PHD3. Although this finding suggests that CpG methylation is involved in silencing, further direct queries of epigenetic alterations at this locus were necessary to more deeply address this question.

### The *PHD3* CpG island is aberrantly CpG methylated and displays decreased chromatin accessibility in human carcinoma cells

To determine whether *PHD3* gene methylation is present at the CpG island in cell lines that have reduced PHD3 mRNA expression and respond to 5-Aza-dC by upregulating PHD3 mRNA, we utilized sodium bisulfite sequencing to identify methylated CpG sites. **Figure 3A**, illustrates the CpG island in the 5'-end of the *PHD3* gene. The 58 CpG sites in the region analyzed are represented by vertical lines. A putative hypoxia response element (HRE) in the promoter region of the gene is also indicated. We found that these CpGs were highly methylated in

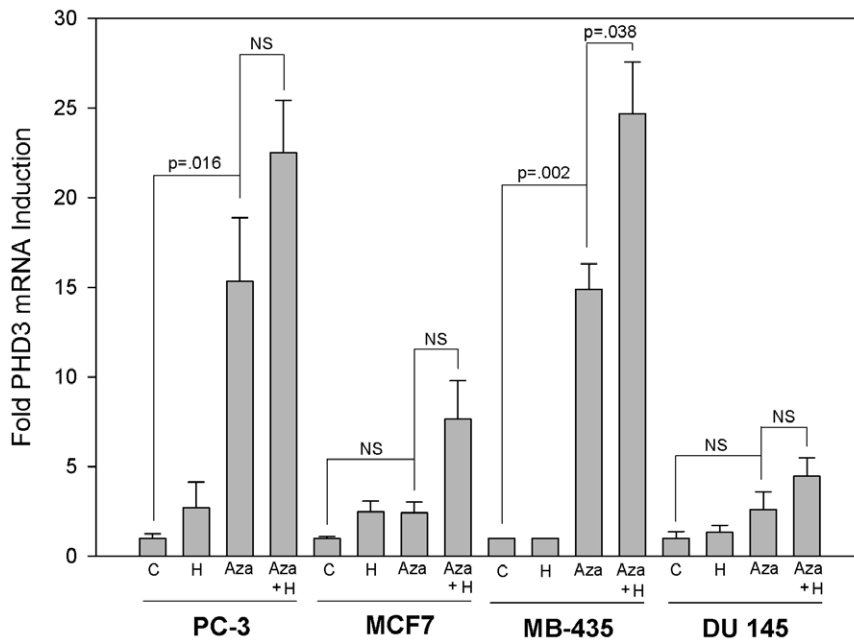


**Figure 2. Treatment with 5-Aza-dC triggers re-expression of PHD3.** Cell lines representative of PHD3 expressers and PHD3 non-expressers were either not treated (C), treated with hypoxia (H), treated with 5-Aza-dC (Aza), or treated with 5-Aza-dC and then subjected to 1% oxygen (Aza + H) according to the protocol described in Materials and Methods. Real time quantitative PCR was performed to determine the mRNA expression of PHD3. The data were normalized to GAPDH and expressed relative to PHD3 mRNA in the corresponding untreated controls. Error bars = SEM. n = 3. doi:10.1371/journal.pone.0014617.g002

the PHD3 negative cell lines PC-3, MB-435, and HS578T (**Figure 3B**). These represent examples of human melanoma, prostate, and mammary carcinoma cells respectively. We also noted that many cell lines appeared to be heterogeneous with respect to *PHD3* promoter methylation status. Within certain cell lines, some clones display high levels of methylation, whereas other have very few to no methylated CpGs. This small population of unmethylated or hemimethylated cells within a cell line may explain our ability to detect very low levels of PHD3 mRNA in cell lines displaying largely methylated *PHD3* CpG islands. Furthermore, areas of CpG methylation in some methylation positive cell lines overlap with a putative HRE in the *PHD3* promoter region, which could hinder the ability of PHD3 to be induced upon hypoxic stimuli. In contrast to the positive methylation status in PHD3 negative cells, the CpGs in the *PHD3* CpG island were largely unmethylated in the PHD3 positive cells, NPrEC, DU 145, 22RV.1, HME1, and MCF7.

DNA methylation is typically associated with other alterations to chromatin structure that participate in cell-type specific gene expression patterns. Aberrant cytosine methylation in the 5'-regulatory regions of genes is typically associated with deacetylated histones, and thus a state of DNA that is generally inaccessible to transcription factors and other enzymes that act on DNA, such as polymerase II. This is a mechanism of gene silencing often exploited by cancer cells [22]. In a chromatin accessibility assay, we found the promoter region of *PHD3* in PC-3 cells was resistant to cutting by DNase I when compared to the MCF7 *PHD3* promoter, whereas there was little change in *GAPDH* promoter accessibility between the two cell lines (**Figure S2**). This evidence further supports the hypothesis that *PHD3* promoter methylation and heterochromatin formation are part of the mechanism for reduced expression of PHD3 in these human breast and prostate cancer cell lines.

#### PHD3 expression is not induced upon exposure to hypoxia in cell lines containing *PHD3* promoter methylation

Unlike *PHD1*, both *PHD2* and *PHD3* genes contain hypoxia response elements, and can be induced by hypoxia by the HIF-1 and HIF-2 transcription factor complex. In the case of *PHD3*, mRNA and protein expression can be relatively low during normoxic conditions, with marked increases upon hypoxic insult [10]. Therefore, we tested PC-3, DU 145, MB-435 and MCF7 cell lines for their ability to upregulate *PHD3* following 24 hours of hypoxia (1% O<sub>2</sub>) (**Figure 4A**). We found cell lines that contained *PHD3* promoter methylation (PC-3, MB-435) failed to appreciably upregulate *PHD3* mRNA under these conditions. However, we did note a very small upregulation of *PHD3* mRNA in PC-3 cells. This can likely be attributed to the heterogeneity of *PHD3* promoter methylation between specific clones in this cell line (see **figure 3B**). In contrast, *PHD3* mRNA was much more prone to upregulation in the unmethylated cell line MCF7. Upregulation of *PHD3* in DU 145 cells varied by experiment, and averaged as a non-significant trend toward hypoxic upregulation.

Our discovery of *PHD3* promoter methylation in melanoma, breast and prostate cancer cell lines prompted us to ask whether cell lines from other malignant tissues contained methylation at the *PHD3* locus. Therefore, we further performed real-time PCR and bisulfite sequencing on a panel of 3 human renal cell carcinoma cell lines (A-498, ACHN and 769-P), and on cDNA prepared from normal kidney tissue (**Figure 4B**). We found that ACHN and 769-P cells express nearly undetectable levels of *PHD3* mRNA, whereas A-498 expresses levels comparable to normal tissue. Of these cell lines, the *PHD3* positive A-498 displayed an unmethylated *PHD3* promoter whereas 769-P cells displayed an aberrantly methylated *PHD3* promoter. Interestingly though, we did not detect any CpG methylation at the promoter of *PHD3* negative

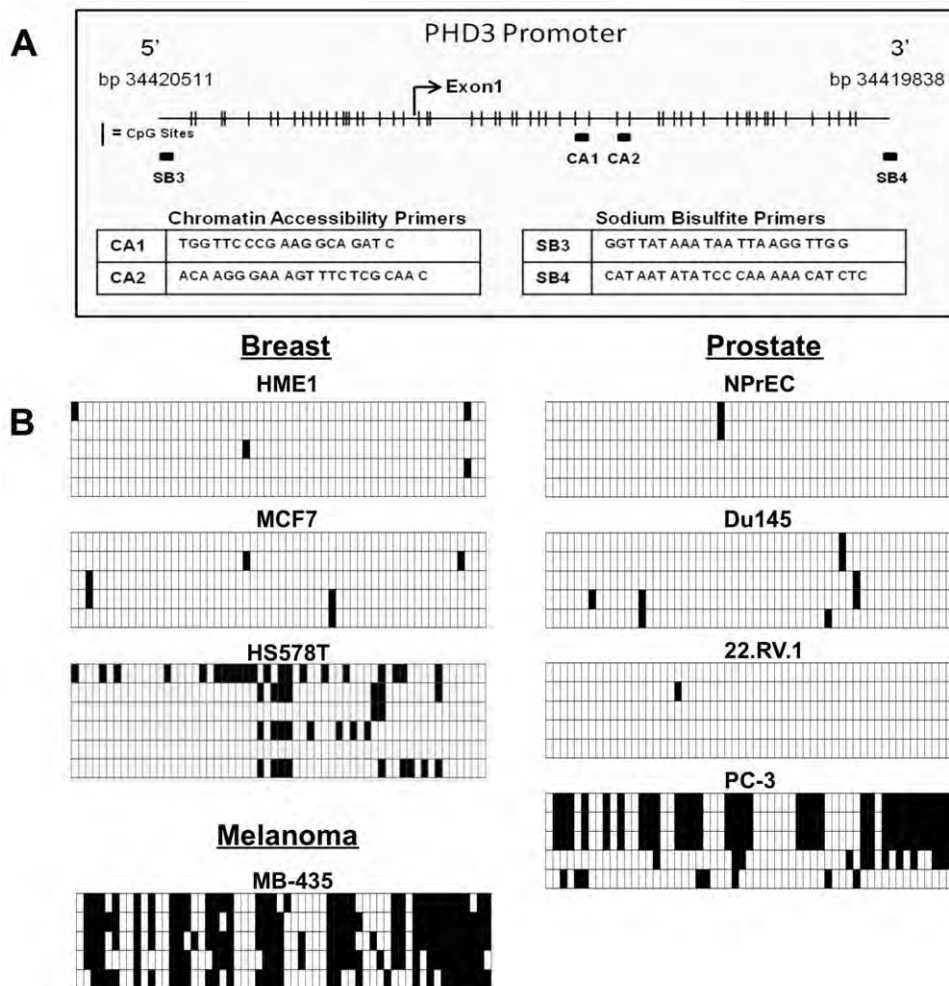


**Figure 3. DNA methylation analysis of the *PHD3* 5'-CpG island in human melanoma, prostate and breast carcinoma cell lines. A)** Schematic representation of the CpG distribution in the 5'-regulatory region of the *PHD3* gene from UCSC Genome Browser coordinates bp34420511-bp34419838. The CpG sites are represented by vertical tick marks, and the beginning of exon 1 is depicted as a bent arrow. The locations of PCR primers used to assess genomic methylation (SB3 and SB4) and chromatin accessibility (CA1 and CA2), respectively. **B)** Bisulfite sequencing was performed on DNA isolated from two non-tumorigenic epithelial cell lines (NPrEC and hTERT-HME1) and six tumor cell lines (DU 145, 22RV.1, PC-3, MB-435, HS578T, and MCF7). Each grid contains at least 5 rows representing the 5 individually cloned and sequenced bisulfite PCR products from the indicated cell lines. Each row contains 58 boxes representing the 58 CpGs in an individual cloned molecule. Open and filled boxes are unmethylated and methylated CpG sites, respectively.  
doi:10.1371/journal.pone.0014617.g003

ACHN cells, suggesting an alternative mechanism for silencing in this cell line.

### *PHD3* promoter methylation status does not correlate with hypoxia induced HIF-1 $\alpha$ protein accumulation or HIF transcriptional activity

The presence of *PHD3* promoter methylation in such a broad range of epithelial malignancies suggests that it may be a selective advantage for tumor survival. One hypothesis is that *PHD3* silencing by promoter methylation may allow for an increased HIF transcriptional response during hypoxic conditions. In order to determine whether *PHD3* promoter methylation specifically affects the hypoxia response pathway, we performed western blots on cell lysates from MCF7, PC-3, MB-435 and DU 145 cell lines to compare the HIF protein levels and the HIF transcriptional response to hypoxia (**Figure 5a**). Following 24 hours of hypoxia, HIF-1 $\alpha$  protein was upregulated in all the cell lines regardless of *PHD3* expression status. We also observed that DU 145 cells appear not to

express detectable levels of *PHD3* protein. We are unsure whether this is due to limits of detection by our *PHD3* antibody, or if DU 145 cells downregulate *PHD3* expression by a posttranslational mechanism. Our antibody appears to be specific to *PHD3* as transduction of an adenoviral-*PHD3* expression vector into PC3 cells produces a band at an identical molecular weight as the band seen in MCF7 cells (**Figure S3**). Interestingly though, MCF7 cells, which do express basal levels of *PHD3* mRNA and protein, displayed the largest induction of HIF-1 $\alpha$  protein. Thus, HIF-1 $\alpha$  protein levels, in general, did not show any correlation with presence or absence of *PHD3*. We also found HIF-2 $\alpha$  to be expressed under normoxic conditions in MCF7. Moreover, MB-435 cells, which express the lowest levels of *PHD3* mRNA out of all the cell lines tested appear not to express HIF-2 $\alpha$  at an appreciable level. Thus, loss of *PHD3* does not appear to be significantly correlated with an accumulation of HIF-1 $\alpha$  or HIF-2 $\alpha$  levels in these cell lines.

To further investigate the effect of *PHD3* promoter methylation on the transcriptional response of the hypoxia response pathway,

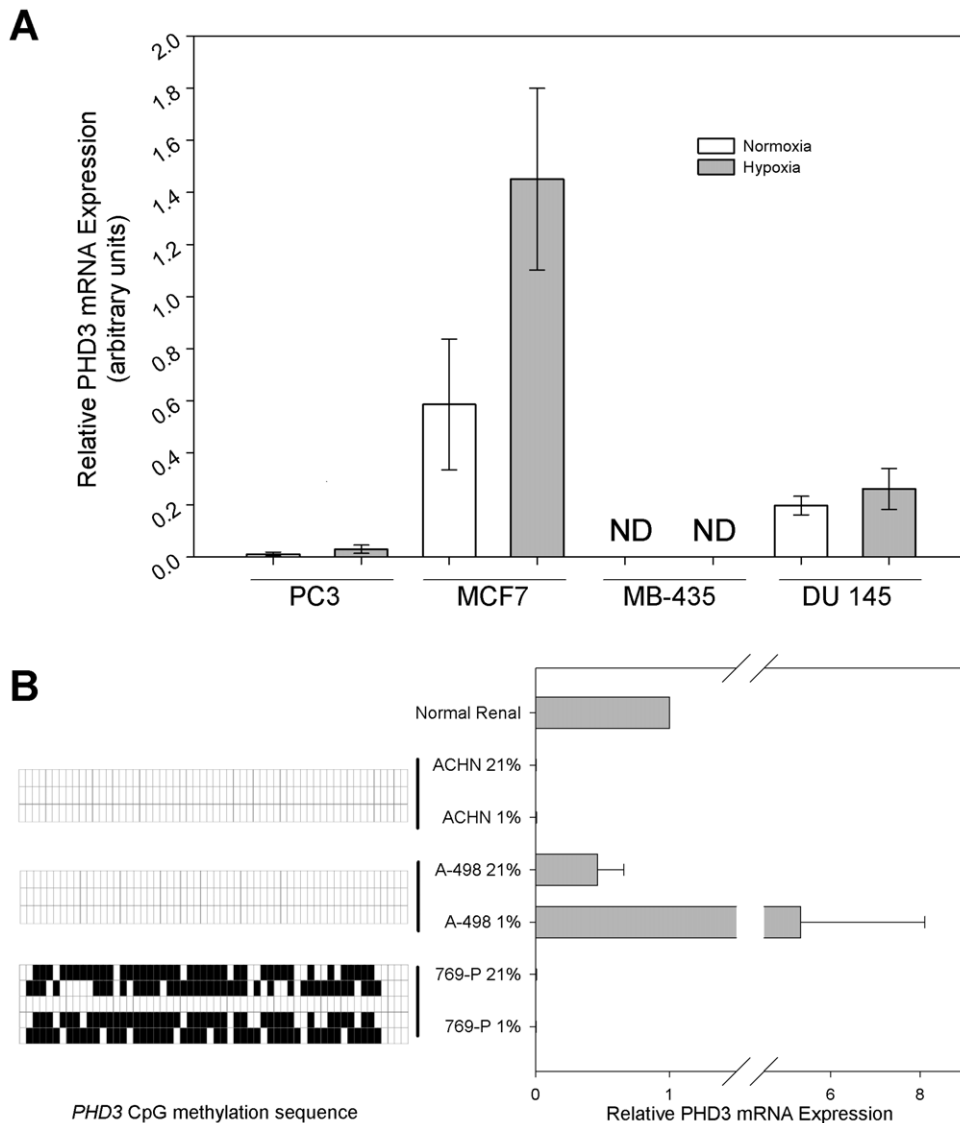


**Figure 4. The methylated *PHD3* gene in melanoma, prostate, breast and renal carcinoma cell lines is refractory to induction by hypoxia.** **A)** Melanoma, prostate and breast carcinoma cell lines were treated with hypoxia (1% O<sub>2</sub>) or normoxia (21% O<sub>2</sub>) for 24 hours. Total RNA was extracted and converted to cDNA by reverse transcription. Quantitative real-time reverse transcription-PCR analysis of *PHD3* was performed with normalization to *GAPDH* gene expression. Relative quantitation was determined by the DDCT method. ND = not detectable. Error bars = SEM. n = 3. **B)** Renal clear cell carcinoma cell lines were either untreated or treated with hypoxia as in A). The right panel depicts relative *PHD3* mRNA levels compared to mRNA extracted from normal renal tissue. The left panel depicts the methylation status at each of 58 CpG dinucleotides present in the *PHD3* CpG island of the representative renal carcinoma cell lines. Error bars = SEM. n = 3. doi:10.1371/journal.pone.0014617.g004

we transfected MCF7, PC-3, MB-435 and DU 145 cancer cell lines with an HRE-luciferase reporter construct [19]. Following 24 hours of hypoxia, luciferase activity was measured and plotted relative to luciferase activity in normoxic cells (**Figure 5B**). There was no correlation between *PHD3* promoter methylation status and hypoxic induction of luciferase. The results of this experiment resembled the pattern of HIF-1 $\alpha$  protein accumulation seen in **figure 5A**. MCF7 cells showed the largest induction luciferase activity, whereas the other cell lines, which do not express detectable levels of *PHD3* protein, were comparable to one another. Although not absolute, these data are highly suggestive that HIF protein stabilization and transcriptional activity is largely independent of *PHD3* expression.

#### *PHD3* promoter methylation is absent in primary human prostate adenocarcinomas

Recent data published by Hatzimichael et al. suggested that acquisition of *PHD3* promoter methylation may be a relatively common event in certain plasma cell neoplasias [17]. Therefore, we asked whether primary human prostate neoplasias contained methylation at the *PHD3* CpG island. We extracted DNA and RNA from frozen sections of 10 prostate cancer specimens containing a minimum of 70% malignant tissue with a Gleason score ranging from 7–9 as well as 3 benign prostate specimens. Real-time PCR of extracted RNA showed that all 10 tumors contained decreased *PHD3* mRNA expression compared to 3 benign tissue specimens (**Figure 6A and B**).

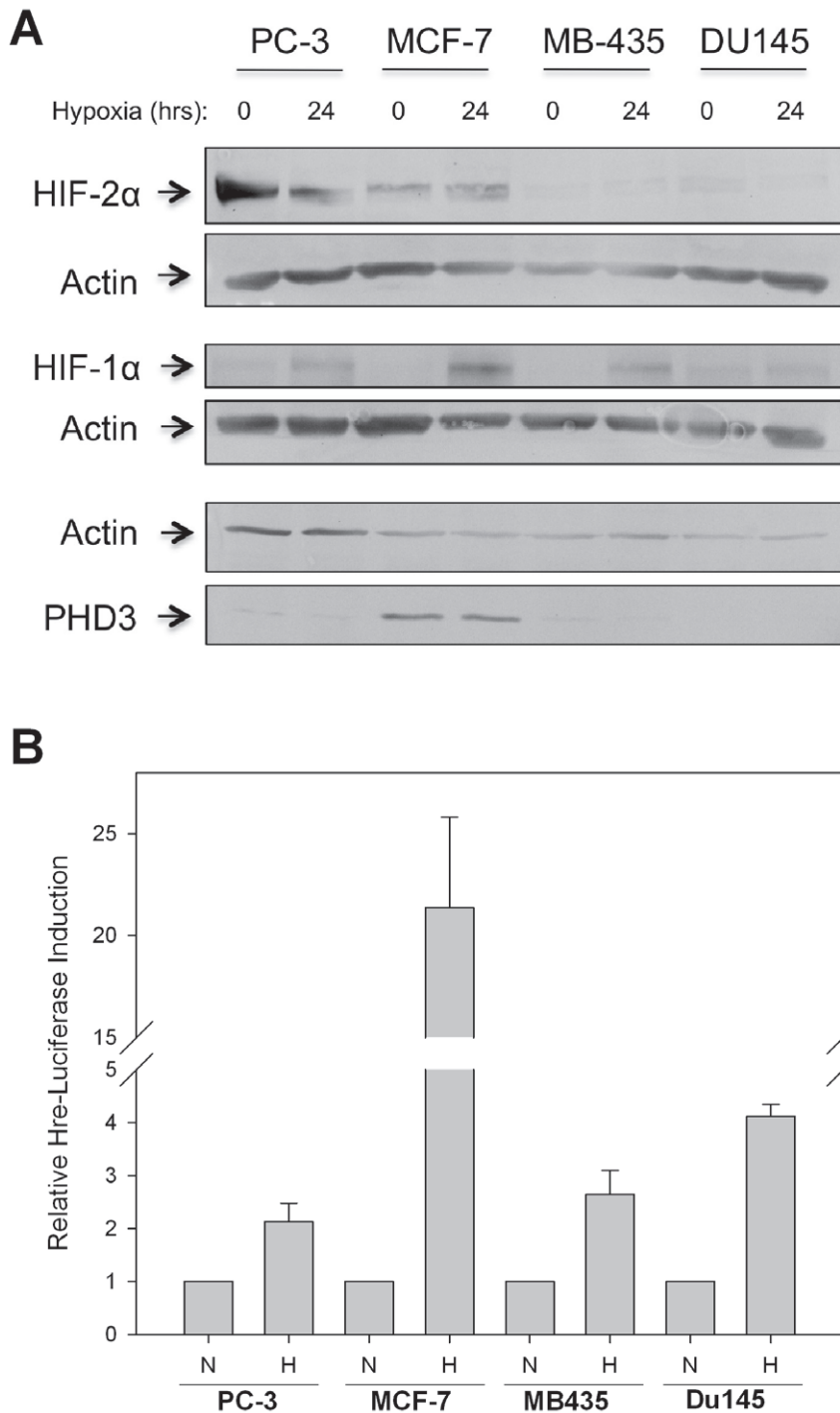


**Figure 5. The HIF-1 response is not impaired in prostate and breast carcinoma cell lines that lack PHD3.** **A)** Melanoma, breast and prostate cancer cell lines with methylated *PHD3* promoters (MB-435, PC-3) and non-methylated promoters (MCF7, DU 145) were subjected to hypoxia (1% O<sub>2</sub>) or normoxia for 24 hours. Thirty micrograms of whole cell lysate was western blotted for the presence of HIF-1 $\alpha$ , HIF-2 $\alpha$  and PHD3; actin was used as a loading control. **B)** Breast and prostate cancer cell lines were transfected with an HRE-luciferase reporter vector and Renilla luciferase vector and then subjected to hypoxia (1% O<sub>2</sub>) or normoxia for 24 hours. Luciferase activities after 24 hours of hypoxia were determined and are depicted relative to luciferase activities in cells under normoxia. Error bars = SEM. n=3 for MCF7 and PC-3. n=2 for MB-435 and DU 145. doi:10.1371/journal.pone.0014617.g005

Probing for methylated CpGs in select tumor specimens using the MethylMiner kit indicated the possible presence of methylated CpGs at the *PHD3* CpG island in tumor sample 1 (Figure S4), which also contained the lowest PHD3 mRNA levels. However, further bisulfite sequencing of 8 clones from

tumor sample 1 and tumor sample 4 did not detect any methylated CpGs (data not shown). This could be due to better sensitivity to population average methylation states as compared to the single molecule at a time approach of bisulfite sequencing.

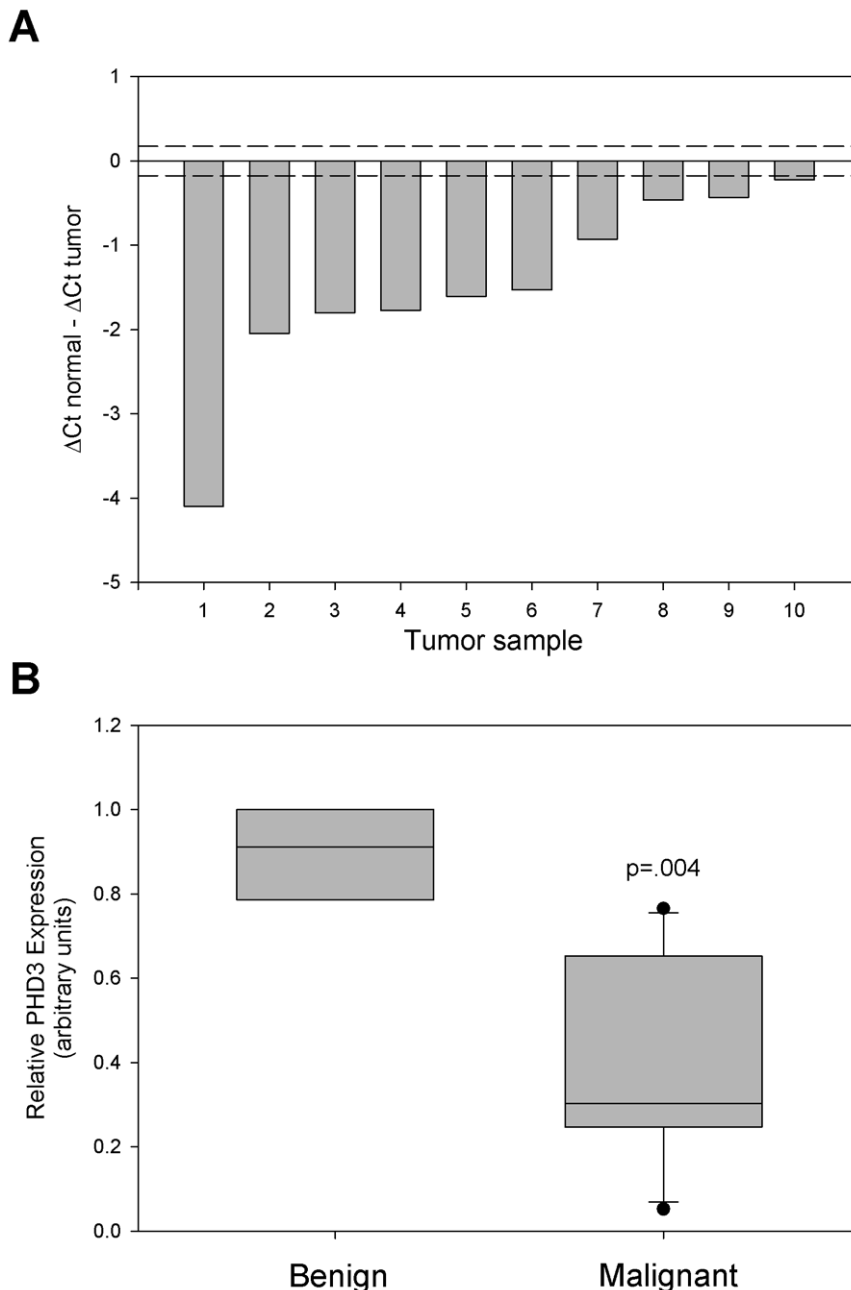


**Figure 6. PHD3 mRNA expression is downregulated in multiple primary human prostate cancer specimens.** **A)** Total mRNA was isolated from frozen sections of primary human prostate cancer specimens with Gleason scores ranging from 7–9. Quantitative real-time PCR was performed using PHD3 specific TaqMan primer-probe. Relative PHD3 mRNA expression for each tumor sample is represented as (average dCt of  $n = 3$  benign prostate tissue samples) – (dCt tumor sample). Samples were normalized to GAPDH. Dotted lines represent  $\pm 1$  SD for benign tissue PHD3 mRNA expression. **B)** Box plot depicting PHD3 mRNA expression from samples shown in A. p value is based on ANOVA between 3 benign samples and 10 malignant samples.  
doi:10.1371/journal.pone.0014617.g006

## Discussion

Perturbations in the cellular responses to hypoxia are well known to play a role in the malignant process. Familial mutations in *VHL*, a negative regulator of the HIF- $\alpha$  proteins, results in vascular tumors of the brain, spinal cord and retina, as well as appearance of renal clear-cell carcinomas [23]. PHD proteins play a role upstream of VHL regulation; they hydroxylate HIF- $\alpha$  proteins, creating a binding site for VHL [24,25,26]. Thus, it is feasible that

deregulation of PHD activity or expression could also contribute to the malignant process. In fact, an absence of PHD3 upregulation following hypoxia has been observed in multiple human cell lines from tumors of the breast, prostate and brain [10,16]. A recent clinical study of breast tumors containing *BRCA* mutations supports the hypothesis that PHD3 plays an important role in malignancy. This study found a positive correlation between decreased PHD3 expression and a basal phenotype, which is considered a higher grade and more aggressive tumor [27].

Here, we report aberrantly silenced basal mRNA expression of PHD3 in breast, prostate, melanoma and renal cell carcinoma cell lines, and the absence of PHD3 mRNA induction upon hypoxic stimulus. PHD3 expression could be recapitulated in some PHD3 negative cell lines after treatment with 5-Aza-dC, a DNA methyltransferase inhibitor, implicating DNA methylation as a mechanism for the decreased expression of PHD3 mRNA in these cell lines. *PHD3* promoter methylation was verified by sequence analysis of PCR products cloned from bisulfite-treated genomic DNA. We found that among the human cancer cell lines investigated, PC-3, MB-435, HS578T, and 769-P cell lines have hypermethylated *PHD3* CpG islands. Furthermore, the *PHD3* promoter region was more resistant to DNase I in PC-3 cells (hypermethylated *PHD3* promoter) compared to MCF7 cells (hypomethylated *PHD3* promoter). The methylation of the *PHD3* promoter in these carcinoma cell lines appears to be aberrant since insignificant DNA methylation was found in the non-transformed cell counterparts of prostate and mammary epithelial cell lines NPrEC and HME1 respectively. The apparently aberrant *PHD3* promoter methylation status in these cell lines is the likely mechanism, at least in part, for PHD3 transcriptional suppression because DNA methylation is typically associated with a condensed heterochromatin state, and is known to inhibit transcription factor binding to promoter regions of genes [28].

Although all members of the PHD family have the ability to hydroxylate both HIF-1 and HIF-2 $\alpha$ , the specificities appear to differ slightly. PHD2 has been reported to play a more pronounced role in the regulation of HIF-1 $\alpha$ , whereas PHD3 more strongly affects HIF-2 $\alpha$  stability [10]. Therefore, it would seem likely that loss of PHD3 expression by promoter methylation would convey a cellular advantage mediated through increased HIF-1 $\alpha$  and/or HIF-2 $\alpha$  stability during hypoxia. This could lead to increased expression of VEGF and erythropoietin with subsequent vascular recruitment. Tumors of the breast, skin, kidney and prostate, being solid tumors, would certainly benefit from an increase in vascular supply to hypoxic areas. In fact, there is evidence that cell lines from other solid tumors downregulate PHD3 as well. Henze et al. have shown that several glioma cell lines display little to no PHD3 protein expression during normoxia, with no induction upon hypoxia when compared to other glioma cell lines studied [16]. Our results would predict that a subset of those cell lines have aberrant methylation of the *PHD3* CpG island. Interestingly, HIF-2 $\alpha$  protein levels after 18 hours of hypoxia appeared lower in PHD3 non-expressing cells than those in cells expressing relatively high levels of PHD3 [16]. This is the opposite of what we had expected, and may demonstrate the ability of other PHD family members to substitute for the loss of PHD3 expression in regulating HIF-1 $\alpha$  and HIF-2 $\alpha$  stability. This hypothesis is supported by data from Appelhoff et al., who measured relative protein amounts of PHD isoforms in multiple cell lines. In cell MB-435 and ZR751 cell lines where PHD3 is low or absent, PHD2 protein is greatly elevated.[29]. Similarly, we found that MCF7 cells, which basally express PHD3 at the mRNA and protein level during normoxic conditions, also express relatively high levels of HIF-2 $\alpha$ . Taken together, we interpret these findings to suggest that *PHD3* silencing by CpG methylation may not have a significant impact on HIF-1 and HIF-2 $\alpha$  protein levels in the cell lines that we tested.

In fact, the results of our study support a mechanism whereby PHD3 silencing by *PHD3* CpG island methylation affects pathways outside of the conventional hypoxic response pathway. When HIF transcriptional activity was measured through a hypoxia responsive HRE-luciferase reporter, we observed nearly equal transcriptional responses to hypoxia in 3 out of 4 cell lines,

which included both PHD3 silenced as well as PHD3 expressing cell lines. In MCF7 cells, which express PHD3 at the protein level and do not contain *PHD3* promoter methylation, we observed nearly a 15-fold increase in luciferase induction upon hypoxic treatment. These results suggest that PHD3 expression status does not significantly affect HIF protein stabilization or HIF transcriptional activity through an HRE containing promoter upon exposure to 1% oxygen. Therefore, modulation of an alternative cellular pathway(s) remains an open candidate for mediating the effects of PHD3 loss in malignancies.

Besides the HIF family proteins, other interacting partners of PHD3 have already been discovered. PHD3 is a known player in both neuronal apoptosis and in myoblast differentiation [30,31] PHD3 also appears to interact with Bcl-2 to induce apoptosis in H9c2 cells in response to doxorubicin [32].Furthermore, PHD3 has also been reported to destabilize ATF-4 through a novel oxygen-dependant domain on ATF-4 [33]. ATF-4 is involved in the regulation of angiogenesis and metabolism [34]. Thus, upregulation of ATF-4 by a loss of PHD3 could promote cell survival. In addition, PHD3 has also been recently reported to inhibit IKK $\beta$ . An increase in IKK $\beta$  activity in the absence of PHD3 could confer a growth advantage to cells through an increase NF $\kappa$ B signaling [35]. Constitutive NF $\kappa$ B activity is an important and common event in T- and B-cell derived malignancies [36,37] and may explain the *PHD3* promoter methylation recently reported in plasma and B-cell neoplasia by Hatzimichael et al. [17]. These interesting prospects related to identification of the downstream targets of PHD3 signaling will undoubtedly become a focus of future investigations.

Our inability to detect *PHD3* promoter DNA methylation in primary human prostate tumors was surprising, however our results are supported by a recent study by Huang et al. [38], who screened 168 invasive breast carcinomas and did not find evidence of *PHD3* DNA methylation using melting curve analysis of bisulfite converted DNA. We cannot rule out the possibility that a low level of semi-methylated *PHD3* CpG islands are present in their samples as the “intermediately methylated” controls were not truly intermediately methylated, but rather were mixtures of 100% methylated DNA with 0% methylated DNA. Nonetheless, it seems clear that a large proportion of primary epithelial tumors does not contain a high degree of *PHD3* promoter methylation, and may not be the ideal specimens for detection of methylation at this locus. Given PHD3’s purported ability to negatively regulate the NF $\kappa$ B pathway [30,35], and the widely reported involvement of NF $\kappa$ B in cell migration and metastasis [39,40], future studies on *PHD3* CpG island methylation in clinical samples of metastatic disease as opposed to primary tumors may yield more positive results.

Here, we are the first to report DNA methylation of the *PHD3* CpG island in solid tumor cell lines derived from diverse cell types. *PHD3* methylation in carcinoma cells was associated with their inability to appropriately upregulate PHD3 mRNA upon exposure to hypoxia. We are also the first to show evidence that this aberrant expression fails to correlate with an increase in HIF protein accumulation and transcriptional activity upon exposure to hypoxia in the cell lines examined. The presence of *PHD3* promoter hypermethylation and PHD3 silencing in such a wide range of cancer types suggests this might be a common event that elicits a selective advantage for tumors. Our data suggest that at least in some cell lines, the nature of this advantage may extend beyond hypoxia resistance. Furthermore, the selective event may occur during or after the process of invasion/metastasis, as we and others have not found evidence of methylation in primary solid tumors [38].

## Supporting Information

**Figure S1** Validation of methylated DNA enrichment as a tool for detecting methylated CpG regions in human genomic DNA. A) Genomic DNA from human melanoma and breast cancer lines was enriched for methylated CpG dinucleotides at the PHD3 CpG island using the MethylMiner kit, followed by quantitative real-time PCR analysis using PHD3 CpG island-specific PCR primers. S = supernatant, representing unmethylated DNA. E1 - E5 represents elutions with 200, 650, 1100, 1550, 2000 mM NaCl respectively. Input = 1/60th total input DNA. Total amounts of eluted DNA from each fraction are represented as a fraction of input (left). Methylated CpG sequences from bisulfite-converted DNA in the corresponding cell lines are depicted for comparison (right). B) Control 100% methylated and 0% methylated oligos supplied by the MethylMiner kit were subjected to the MethylMiner protocol. S = supernatant, representing unmethylated DNA. E1-E5 represent elutions with 200, 650, 1100, 1550, 2000 mM NaCl respectively. Identical volumes of DNA from each eluate were subjected to quantitative real-time PCR using primers supplied by the MethylMiner kit. DNA content in each fraction is represented as arbitrary units.

Found at: doi:10.1371/journal.pone.0014617.s001 (10.36 MB TIF)

**Figure S2** The methylated PHD3 gene in non-expressing cells is maintained in a less accessible state than the non-methylated PHD3 gene in expressing cells. A) Nuclei from PHD3-positive MCF7 and PHD3-negative PC-3 carcinoma cell lines were isolated and enzymatically restricted with DNase I. Primers CA1 and CA2 (see Fig. 3A) were used for quantitative real-time PCR (right panels) to amplify a region also assessed for cytosine methylation. Accessibility indices (left panels) were calculated as follows:  $AI = 2((Ct\ DNase\ treated) - (Ct\ Untreated))$ . B) GAPDH accessibility indices were simultaneously assessed as a control for a constitutively expressed gene in both cell lines.

Found at: doi:10.1371/journal.pone.0014617.s002 (3.00 MB TIF)

**Figure S3** PHD3 antibody specificity. PC3 cells were transduced with an increasing MOI of adenoviral-PHD3 vector. Western blot using Novus100-139 antibody co-incubated with anti-actin antibody indicated an approximately 27 kDa band in MCF7 cells that migrates at the same molecular weight as a band present in PHD3 transduced PC3 cells.

Found at: doi:10.1371/journal.pone.0014617.s003 (3.00 MB TIF)

## References

- Pasanen A, Heikkilä M, Rautavuoma K, Hirsilä M, Kivirikko KI, et al. Hypoxia-inducible factor (HIF)-3 $\alpha$  is subject to extensive alternative splicing in human tissues and cancer cells and is regulated by HIF-1 but not HIF-2. *Int J Biochem Cell Biol* 42: 1189–1200.
- Semenza GL (2003) Targeting HIF-1 for cancer therapy. *Nat Rev Cancer* 3: 721–732.
- Huang LE, Bunn HF (2003) Hypoxia-inducible factor and its biomedical relevance. *J Biol Chem* 278: 19575–19578.
- Hu CJ, Wang LY, Chodosh LA, Keith B, Simon MC (2003) Differential roles of hypoxia-inducible factor 1 $\alpha$  (HIF-1 $\alpha$ ) and HIF-2 $\alpha$  in hypoxic gene regulation. *Mol Cell Biol* 23: 9361–9374.
- Dery MA, Michaud MD, Richard DE (2005) Hypoxia-inducible factor 1: regulation by hypoxic and non-hypoxic activators. *Int J Biochem Cell Biol* 37: 535–540.
- Ohh M, Park CW, Ivan M, Hoffman MA, Kim TY, et al. (2000) Ubiquitination of hypoxia-inducible factor requires direct binding to the beta-domain of the von Hippel-Lindau protein. *Nat Cell Biol* 2: 423–427.
- Ema M, Taya S, Yokotani N, Sogawa K, Matsuda Y, et al. (1997) A novel bHLH-PAS factor with close sequence similarity to hypoxia-inducible factor 1 $\alpha$  regulates the VEGF expression and is potentially involved in lung and vascular development. *Proc Natl Acad Sci U S A* 94: 4273–4278.
- Wang GL, Jiang BH, Rue EA, Semenza GL (1995) Hypoxia-inducible factor 1 is a basic-helix-loop-helix-PAS heterodimer regulated by cellular O<sub>2</sub> tension. *Proc Natl Acad Sci U S A* 92: 5510–5514.
- Epstein AC, Gleadle JM, McNeill LA, Hewitson KS, O'Rourke J, et al. (2001) C. elegans EGL-9 and mammalian homologs define a family of dioxygenases that regulate HIF by prolyl hydroxylation. *Cell* 107: 43–54.
- Appelhoff RJ, Tian YM, Raval RR, Turley H, Harris AL, et al. (2004) Differential function of the prolyl hydroxylases PHD1, PHD2, and PHD3 in the regulation of hypoxia-inducible factor. *J Biol Chem* 279: 38458–38465.
- Metzen E, Berchner-Pfannschmidt U, Stengel P, Marxsen JH, Stolze I, et al. (2003) Intracellular localisation of human HIF-1 $\alpha$  hydroxylases: implications for oxygen sensing. *J Cell Sci* 116: 1319–1326.
- Tuckerman JR, Zhao Y, Hewitson KS, Tian YM, Pugh CW, et al. (2004) Determination and comparison of specific activity of the HIF-prolyl hydroxylases. *FEBS Lett* 576: 145–150.
- Uchida T, Rossignol F, Matthey MA, Mounier R, Couette S, et al. (2004) Prolonged hypoxia differentially regulates hypoxia-inducible factor (HIF)-1 $\alpha$  and HIF-2 $\alpha$  expression in lung epithelial cells: implication of natural antisense HIF-1 $\alpha$ . *J Biol Chem* 279: 14871–14878.
- Berra E, Benizri E, Ginouves A, Volmat V, Roux D, et al. (2003) HIF prolyl-hydroxylase 2 is the key oxygen sensor setting low steady-state levels of HIF-1 $\alpha$  in normoxia. *Embo J* 22: 4082–4090.

**Figure S4** Methylated DNA enrichment of genomic DNA isolated from primary human prostate cancer. A) Total genomic DNA was isolated from frozen sections of 7 malignant prostate cancers and 3 benign prostate samples and subjected to the MethylMiner protocol. Tumor sample number corresponds to samples shown in figure 6A. S = supernatant, representing unmethylated DNA. E1-E4 represents elutions with 300, 550, 800, and 2000 mM NaCl. PHD3 CpG island DNA content in each fraction is represented as a fraction of total PHD3 CpG island DNA present in input.

Found at: doi:10.1371/journal.pone.0014617.s004 (8.41 MB TIF)

## Acknowledgments

The authors are indebted to the late Professor Larry Oberley for his pioneering contributions to this work. We thank Dr. Robert Freeman (Rochester University) for his gracious gift of the adenoviral-PHD3 construct. We also thank Suwimol Kaewpila for expert technical assistance.

## Author Contributions

Conceived and designed the experiments: FED. Performed the experiments: TLP MPF SV SUV AJC MLT. Analyzed the data: TLP MPF FED. Contributed reagents/materials/analysis tools: AJC MLT. Wrote the paper: TLP FED. Assisted with writing and editing: TLP MPF SUV. Provided funding resources for the work: SV MLT AJC FED. Isolated proteins from human tumor samples and all cell lines under normoxia and hypoxia; performed transfection studies for promoter reporter experiments; performed bisulfite sequencing and methylminer experiments and provided key data for figures 6a (right panel) and 6b: TLP. Extracted, quantified, and analyzed RNA and DNA from all cell lines; designed primers and performed bisulfite sequencing to determine methylation patterns. Provided key data for figures 1, 3, and 4: MPF. Extracted RNA, DNA and protein from breast cancer cell lines treated with 5-aza-dC for initial RT-PCR and western blotting experiments; provided key data for figures 1, 2, 5: SV. Extracted RNA, DNA and protein from human cell lines and tumor samples, performed bisulfite and Methylminer experiments on cell lines and tumor samples and assisted with producing real time PCR replicate data for PHD3 expression experiments: SUV. Extracted RNA and protein from prostate and renal cell lines for initial RT-PCR and western blotting experiments; provided key data for parts of figures 1 and 3: AJC. Isolated proteins for western blotting; provided reagents and expertise for western blots and trained the other authors in protein techniques; provided key data for figure 6a (left panel): MLT. Provided overall guidance and direction in all phases of experimental design, implementation, data acquisition and interpretation, and manuscript writing, editing and preparation: FED.

15. Nakayama K, Frew IJ, Hagensen M, Skals M, Habelhah H, et al. (2004) Siah2 regulates stability of prolyl-hydroxylases, controls HIF1alpha abundance, and modulates physiological responses to hypoxia. *Cell* 117: 941–952.
16. Henze AT, Riedel J, Diem T, Wenner J, Flamme I, et al. Prolyl hydroxylases 2 and 3 act in gliomas as protective negative feedback regulators of hypoxia-inducible factors. *Cancer Res* 70: 357–366.
17. Hatzimichael E, Dasoula A, Shah R, Syed N, Papoudou-Bai A, et al. (2009) The prolyl-hydroxylase EGLN3 and not EGLN1 is inactivated by methylation in plasma cell neoplasia. *Eur J Haematol*.
18. Rose SL, Fitzgerald MP, White NO, Hitchler MJ, Futscher BW, et al. (2006) Epigenetic regulation of maspin expression in human ovarian carcinoma cells. *Gynecol Oncol* 102: 319–324.
19. Salnikow K, An WG, Melillo G, Blagosklonny MV, Costa M (1999) Nickel-induced transformation shifts the balance between HIF-1 and p53 transcription factors. *Carcinogenesis* 20: 1819–1823.
20. Domann FE, Futscher BW (2004) Flipping the epigenetic switch. *Am J Pathol* 164: 1883–1886.
21. Momparler RL (2005) Pharmacology of 5-Aza-2'-deoxycytidine (decitabine). *Semin Hematol* 42: S9–16.
22. Szyf M (2005) DNA methylation and demethylation as targets for anticancer therapy. *Biochemistry (Mosc)* 70: 533–549.
23. Maher ER, Kaelin WG, Jr. (1997) von Hippel-Lindau disease. *Medicine (Baltimore)* 76: 381–391.
24. Ivan M, Kondo K, Yang H, Kim W, Valiando J, et al. (2001) HIF1alpha targeted for VHL-mediated destruction by proline hydroxylation: implications for O2 sensing. *Science* 292: 464–468.
25. Jaakkola P, Mole DR, Tian YM, Wilson MI, Gielbert J, et al. (2001) Targeting of HIF-1alpha to the von Hippel-Lindau ubiquitylation complex by O2-regulated prolyl hydroxylation. *Science* 292: 468–472.
26. Yu F, White SB, Zhao Q, Lee FS (2001) HIF-1alpha binding to VHL is regulated by stimulus-sensitive proline hydroxylation. *Proc Natl Acad Sci U S A* 98: 9630–9635.
27. Yan M, Rayoo M, Takano EA, Thorne H, Fox SB (2009) BRCA1 tumours correlate with a HIF-1alpha phenotype and have a poor prognosis through modulation of hydroxylase enzyme profile expression. *Br J Cancer* 101: 1168–1174.
28. Cyr A, Domann F. The Redox Basis of Epigenetic Modifications: From Mechanisms to Functional Consequences. *Antioxid Redox Signal*.
29. Appelhoff RJ, Tian Y-M, Raval RR, Turley H, Harris AL, et al. (2004) Differential function of the prolyl hydroxylases PHD1, PHD2, and PHD3 in the regulation of hypoxia-inducible factor. *J Biol Chem*. pp 38458–38465.
30. Fu J, Taubman MB. Prolyl hydroxylase EGLN3 regulates skeletal myoblast differentiation through an NF-kappaB-dependent pathway. *J Biol Chem* 285: 8927–8935.
31. Lipscomb EA, Sarmiere PD, Freeman RS (2001) SM-20 is a novel mitochondrial protein that causes caspase-dependent cell death in nerve growth factor-dependent neurons. *J Biol Chem* 276: 5085–5092.
32. Liu Y, Huo Z, Yan B, Lin X, Zhou ZN, et al. Prolyl hydroxylase 3 interacts with Bcl-2 to regulate doxorubicin-induced apoptosis in H9c2 cells. *Biochem Biophys Res Commun* 401: 231–237.
33. Koditz J, Nesper J, Wottawa M, Stiehl DP, Camenisch G, et al. (2007) Oxygen-dependent ATF-4 stability is mediated by the PHD3 oxygen sensor. *Blood* 110: 3610–3617.
34. Ameri K, Harris AL (2008) Activating transcription factor 4. *Int J Biochem Cell Biol* 40: 14–21.
35. Xue J, Li X, Jiao S, Wei Y, Wu G, et al. (2009) Prolyl Hydroxylase-3 Is Down-regulated in Colorectal Cancer Cells and Inhibits IKKbeta Independent of Hydroxylase Activity. *Gastroenterology*.
36. Jost PJ, Ruland J (2007) Aberrant NF-kappaB signaling in lymphoma: mechanisms, consequences, and therapeutic implications. *Blood* 109: 2700–2707.
37. Annunziata CM, Davis RE, Demchenko Y, Bellamy W, Gabrea A, et al. (2007) Frequent engagement of the classical and alternative NF-kappaB pathways by diverse genetic abnormalities in multiple myeloma. *Cancer Cell* 12: 115–130.
38. Huang KT, Mikeska T, Dobrovic A, Fox SB. DNA methylation analysis of the HIF-1alpha prolyl hydroxylase domain genes PHD1, PHD2, PHD3 and the factor inhibiting HIF gene FIH in invasive breast carcinomas. *Histopathology*.
39. Kim A, Kim MJ, Yang Y, Kim JW, Yeom YI, et al. (2009) Suppression of NF-kappaB activity by NDRG2 expression attenuates the invasive potential of highly malignant tumor cells. *Carcinogenesis* 30: 927–936.
40. Maier HJ, Schmidt-Strassburger U, Huber MA, Wiedemann EM, Beug H, et al. NF-kappaB promotes epithelial-mesenchymal transition, migration and invasion of pancreatic carcinoma cells. *Cancer Lett* 295: 214–228.



## Original Contribution

## Elevated mitochondrial superoxide disrupts normal T cell development, impairing adaptive immune responses to an influenza challenge

Adam J. Case<sup>a</sup>, Jodi L. McGill<sup>b</sup>, Lorraine T. Tygrett<sup>b</sup>, Takuji Shirasawa<sup>c</sup>, Douglas R. Spitz<sup>a</sup>, Thomas J. Waldschmidt<sup>b</sup>, Kevin L. Legge<sup>b</sup>, Frederick E. Domann<sup>a,\*</sup><sup>a</sup> Free Radical and Radiation Biology Program, Department of Radiation Oncology, Carver College of Medicine, Holden Comprehensive Cancer Center, The University of Iowa, Iowa City, IA 52242, USA<sup>b</sup> Department of Pathology, Carver College of Medicine, The University of Iowa, Iowa City, IA 52242, USA<sup>c</sup> Department of Aging Control Medicine, Juntendo University, Bunkyo-ku, Tokyo 113-0033, Japan

## ARTICLE INFO

## Article history:

Received 17 August 2010

Revised 12 November 2010

Accepted 22 November 2010

Available online 2 December 2010

## Keywords:

Superoxide

Manganese superoxide dismutase

Cre/loxP

Transgenic

Mouse

Adaptive immunity

Developmental biology

Influenza

Antioxidants

Apoptosis

Immunodeficiency

Free radicals

## ABSTRACT

Reactive oxygen species (ROS) are critical in a broad spectrum of cellular processes including signaling, tumor progression, and innate immunity. The essential nature of ROS signaling in the immune systems of *Drosophila* and zebrafish has been demonstrated; however, the role of ROS, if any, in mammalian adaptive immune system development and function remains unknown. This work provides the first clear demonstration that thymus-specific elevation of mitochondrial superoxide ( $O_2^{\cdot-}$ ) disrupts normal T cell development and impairs the function of the mammalian adaptive immune system. To assess the effect of elevated mitochondrial superoxide in the developing thymus, we used a T-cell-specific knockout of manganese superoxide dismutase (i.e., SOD2) and have thus established a murine model to examine the role of mitochondrial superoxide in T cell development. Conditional loss of SOD2 led to increased superoxide, apoptosis, and developmental defects in the T cell population, resulting in immunodeficiency and susceptibility to the influenza A virus H1N1. This phenotype was rescued with mitochondrially targeted superoxide-scavenging drugs. These findings demonstrate that loss of regulated levels of mitochondrial superoxide lead to aberrant T cell development and function, and further suggest that manipulations of mitochondrial superoxide levels may significantly alter clinical outcomes resulting from viral infection.

© 2010 Elsevier Inc. All rights reserved.

The term reactive oxygen species (ROS) describes a large group of free radical and non-free radical oxygen-containing compounds (e.g., superoxide,  $O_2^{\cdot-}$ ; hydrogen peroxide,  $H_2O_2$ ; peroxynitrite, ONOO<sup>-</sup>; hydroxyl radical,  $\cdot OH$ ) [1]. It is commonly accepted that ROS are by-products of normal metabolism and as such act to damage cellular components such as nucleic acids, proteins, or lipids [2–4]. Because of this, ROS have been implicated in many different diseases including cancer, atherosclerosis, amyotrophic lateral sclerosis, Alzheimer disease, and many others [5–8]. One specific role of ROS is their ability to enhance the pathogenesis of infections, such as influenza

[9,10]. It has been demonstrated that during times of influenza infection ROS may damage lung parenchyma cells, but that this injury may be ameliorated by antioxidant supplementation [11–14]. Current theories propose the mechanism behind this benefit to be attenuation of ROS produced by the innate immune system, but this is not commonly accepted and is still highly debated. More recently it has been shown that cells possess the ability to exploit ROS for signaling and functional purposes. For example, many transcription factor pathways are sensitive to oxidative stress and as such are able to help cells adapt to large deviations in redox status [15–18]. Moreover, ROS are essential in the development of certain organ systems and even whole organisms [19,20]. With this knowledge, the importance of ROS in biology is being elucidated, but many questions about tissue-specific dependence, specific ROS functions, molecular targets of ROS, and ROS mechanisms of action remain unanswered.

One organ system in which ROS have been widely described is the immune system. The biological relevance of ROS in this system was first depicted when it was found that leukocytes generated ROS during the oxidative burst to neutralize pathogens [21]. More recent studies have demonstrated the importance of ROS in the downstream intracellular signaling post-T-cell activation [22–24].

**Abbreviations:** ROS, reactive oxygen species;  $O_2^{\cdot-}$ , superoxide; SOD2, manganese superoxide dismutase; IAV, influenza A virus; ONOO<sup>-</sup>, peroxynitrite;  $\cdot OH$ , hydroxyl radical; SOD1, copper/zinc superoxide dismutase; SOD3, extracellular superoxide dismutase; SOD2<sup>-/-</sup>, conditional SOD2 knockout mouse; SOD2<sup>LoxP</sup>, control loxP-containing mouse; DHE, dihydroethidium; DCFH-DA, dihydrodichlorofluorescein diacetate; RNS, reactive nitrogen species; TEM, transmission electron microscopy; Lck, lymphocyte-specific kinase; IFN- $\gamma$ , interferon- $\gamma$ ; TNF- $\alpha$ , tumor necrosis factor- $\alpha$ ; NBT, nitroblue tetrazolium; MFI, mean fluorescence intensity; HBSS, Hanks' buffered salt solution; PBS, phosphate-buffered saline.

\* Corresponding author. Fax: +1 319 335 8039.

E-mail address: [frederick-domann@uiowa.edu](mailto:frederick-domann@uiowa.edu) (F.E. Domann).

Furthermore, evidence has shown that hydrogen peroxide acts as an important chemoattractant to direct leukocytes to wound margins at sites of injury, which was pivotal in demonstrating that immune cells are able to respond to exogenous ROS in addition to producing endogenous levels [25]. Recent studies have demonstrated the role of ROS in priming the development of the primitive immune system in *Drosophila*, illuminating the first described function of ROS in the development of this organ system in an invertebrate species [26]. Finally, it has been demonstrated that an intracellular pro-oxidant shift occurs before normal thymocyte apoptosis during selection [27], and numerous groups have shown increased ROS levels in pathologic T cell systems [28–30]. In contrast, few studies to date have focused on how pro- or antioxidants affect the normal mammalian adaptive immune system, and to our knowledge no published studies have directly addressed the role of excess mitochondrial superoxide in the growth or function of the adaptive immune system. With the understanding that ROS play a major part in intracellular signaling and cellular damage, we hypothesized that mitochondrial superoxide may play a distinct role in normal development and maintenance of the mammalian adaptive immune system, which could be central to intercellular communication between the innate and the adaptive branches of the immune system.

Although the conceptual framework underlying this hypothesis seems simple in nature, the availability of animal models with which to address this hypothesis is limited. Numerous constitutive antioxidant enzyme knockout animals have provided valuable information on the global developmental importance of these proteins [31–36], but these studies have not assessed the role of specific ROS in tissue-specific adaptive immunity. To address these deficits, we used a conditional T cell manganese superoxide dismutase (i.e., SOD2) knockout mouse to examine the role of increased steady-state levels of superoxide during mammalian adaptive immune system development [37]. The superoxide dismutase class of enzymes specifically scavenges superoxide in biological systems [38]. Mammals contain three variants of the enzymes: cytoplasmic Cu/Zn SOD, SOD1; mitochondrial SOD2; and extracellular SOD, SOD3. Because SOD2 has the explicit role of eliminating mitochondrial superoxide, tissue-specific disruption of this activity should provide an excellent *in vivo* model under conditions where compartmentalized superoxide metabolism is disrupted. A constitutive SOD2 knockout mouse has been created, but because of the postnatal developmental dependence on SOD2 the animal succumbs to numerous organ failures shortly after birth [39,40]. Furthermore, because of the mouse's limited life span no examination of the immune system was reported. Taken together, our model serves as the first described animal model for studying the effects of perturbing steady-state mitochondrial superoxide levels on the development and function of the mammalian T cell adaptive immune system.

## Materials and methods

### Mice

Mice homozygous for the floxed SOD2 allele (i.e., B6.Cg-*Sod2*<sup>tm1</sup>, shorthand SOD2<sup>L/L</sup>), in which exon 3 of the SOD2 gene is flanked by two loxP sequences, have been previously described [37]. B6.Cg-Tg-*Lck-Cre*<sup>548jxm</sup>/J, or Lck-Cre, mice (in which Cre recombinase is exogenously expressed under the control of the proximal lymphocyte-specific kinase and Cre recombinase becomes activated in  $\alpha\beta$  T cells during the CD4<sup>-</sup>/CD8<sup>-</sup> to CD4<sup>+</sup>/CD8<sup>+</sup> stage of development) and B6.Cg-Tg-*Vav1-iCre*<sup>A2Kio</sup>/J, or Vav-iCre, mice (Cre recombinase is exogenously expressed under control of the Vav promoter, and Cre recombinase becomes activated within the hematopoietic stem cell and affects all lymphoid, myeloid, and erythroid lineages) were generously donated by Dr. Adam Dupuy (The University of Iowa) and have been

previously described [41,42]. B6.Cg-Tg-*AlbCre*<sup>21Mgn</sup>/J mice (Cre recombinase is exogenously expressed under the control of the albumin promoter and as such expression is limited to the liver) were generously donated by Dr. Curt Sigmund (The University of Iowa) and have been previously described [43]. Finally, B6.129-Tg-*MMTVCre*<sup>4Mam</sup>/J mice (Cre recombinase is exogenously expressed under the control of the mouse mammary tumor virus promoter, and expression is primarily limited to mammary tissue) were purchased from The Jackson Laboratory and have been previously described [44]. To obtain conditional T cell SOD2 homozygous knockout animals (i.e., SOD2<sup>-/-</sup>), parent strains of both the floxed SOD2 and the Lck-Cre mice were bred to generate F1 heterozygotes (i.e., SOD2<sup>wt/-</sup>). The F1 generation was then bred back to the parent floxed SOD2 mice to create F2 homozygous knockouts. Lck-Cre was passed only through male parents to limit nonspecific oocyte expression. The mice used were of pure C57BL/6 background, and littermate floxed animals (i.e., SOD2<sup>L/L</sup>) served as controls. All work was performed under the approval of the Institutional Animal Care and Use Committee at The University of Iowa.

### Tissue isolation

For all experiments, fresh tissue was harvested and used from animals at 6 weeks of age unless otherwise noted. For thymocyte, splenocyte, and lymph node preps, organs were freshly harvested upon necropsy and placed in a solution of Hanks' buffered salt solution (HBSS) containing 10% fetal bovine serum. Tissues were dissociated by physical disruption using ground glass. After this, lymphocytes were isolated by mouse optimized FicoLite-LM gradient (Atlanta Biologicals, Atlanta, GA, USA). Remaining red blood cell contaminants were removed by red blood cell lysis buffer, and the remaining lymphocytes were washed twice with PBS before further analysis. Peripheral blood was isolated by retro-orbital bleeding into heparin-coated capillary tubes.

### Real-time PCR

RNA was extracted using the Trizol method and was quantified by the use of a Nanodrop ND-1000. One microgram from each sample was reverse transcribed using the ABI cDNA archive kit. Generated cDNA was then subjected to SYBR green quantitative real-time PCR with primers specific to each individual transcript and the 18 S control (supplementary primer sequences) under the following PCR parameters: 95 °C for 10 min, followed by 35 cycles of 95 °C for 15 s and 60 °C for 1 min. A threshold in the linear range of PCR amplification was selected and the cycle threshold (C<sub>t</sub>) determined. Levels of transcripts were then normalized to the 18 S control and compared relative to the SOD2<sup>L/L</sup> control using the  $\Delta\Delta C_t$  method.

### Western blot analysis

Protein was extracted using standard RIPA buffer and was quantified on the basis of the Bradford assay and a standard curve. Protein was run on an SDS-PAGE gel for separation of different-sized proteins. The products were then transferred from the gel to a nitrocellulose membrane. Identification and quantification of the amount of protein were performed by addition of specific primary antibody and then the addition of a horseradish peroxidase-tagged secondary antibody to the first. Chemiluminescent substrate was added to the blot for exposure of products, and film was exposed and qualitatively quantified for protein amount. Loading errors were controlled for by normalizing to  $\beta$ -actin. Antibodies used for this study were SOD2 (Millipore, Billerica, MA, USA), aconitase (Abcam, Cambridge, MA, USA), SDHB (Abcam), LC3 (Cell Signaling Technology, Beverly, MA, USA), p53 (Abcam), and  $\beta$ -actin (Abcam).

### SOD2 activity

To analyze the activity of the superoxide dismutase enzymes, the indirect competitive inhibition assay developed by Spitz and Oberley was used [45]. Briefly, superoxide is generated from xanthine by xanthine oxidase and detected by recording the reduction of nitroblue tetrazolium (NBT). SOD scavenges superoxide and competitively inhibits the reduction of NBT. One unit of SOD activity is defined as the amount of protein required to inhibit 50% of the maximal NBT reduction. To obtain the amount of MnSOD activity, sodium cyanide (5 mmol/L) is added to inhibit the CuZnSOD enzyme activity.

### Dihydroethidium/dichlorofluorescein diacetate staining

Superoxide-specific dihydroethidium (DHE) analysis was performed as previously described [46]. Briefly, superoxide production was estimated using the fluorescent dye DHE from Molecular Probes (Eugene, OR, USA). Cells were washed once with PBS and labeled in suspension at 37 °C for 45 min in PBS (containing 5 mmol/L pyruvate) with DHE (10 μmol/L; in 1% dimethyl sulfoxide (DMSO)). Samples were analyzed using an LSR flow cytometer (superoxide-specific excitation 405 nm, emission 585 nm, band-pass filter; nonspecific excitation 488 nm, emission 585 nm, band-pass filter). The mean fluorescence intensity (MFI) of 10,000 cells was analyzed in each sample and corrected for autofluorescence from unlabeled cells. Dihydrodichlorofluorescein diacetate (DCFH-DA) analysis was performed as previously described [47]. Briefly, steady-state levels of prooxidants were determined using the peroxide oxidation-sensitive (CDCFH<sub>2</sub>, 10 μg/ml) and oxidation-insensitive (CDCF, 10 μg/ml) fluorescent dyes (dissolved in 1% DMSO) obtained from Molecular Probes. The cells were washed once with PBS and labeled with the fluorescent dyes for 15 min at 37 °C in PBS. The cells then were then resuspended in PBS and analyzed using an LSR flow cytometer (excitation 488 nm, emission 530 nm, band-pass filter). The MFI of 10,000 cells was analyzed in each sample and corrected for autofluorescence from unlabeled cells.

### Aconitase and succinate dehydrogenase activities

Aconitase activity assay was adapted from the previously described experiment [48]. Briefly, protein from freshly isolated thymocytes was isolated by sequential freeze/thaws (3×) in a Tris/MnCl<sub>2</sub>/citrate buffer (50 mM Tris, 600 μM MnCl<sub>2</sub>, and 5 mM Na citrate). Protein was then quantified by the Bradford assay. After this, 200 μg protein was combined with NADP<sup>+</sup> (200 μM) and isocitrate dehydrogenase (10 units). Reaction was monitored at 340 nm for the appearance of NADPH formed every 5 min for 2 h. Rates were determined from slopes determined by regression analysis of data. Succinate dehydrogenase activity assay was adapted from the previously described experiment [49]. Briefly, protein from freshly isolated thymocytes was isolated by sequential freeze/thaws (3×) in a phosphate buffer (20 mM). Protein was then quantified by the Bradford assay. After this, 200 μg protein was combined with succinate, non-complex II inhibitors (antimycin A, rotenone, and cyanide), CoQ, and 2,6-dichloroindophenol (DCIP). Reaction was monitored at 600 nm for the colorimetric change in DCIP accepting electrons every 5 min for 1 h. Rates were determined from slopes determined by regression analysis of data.

### Electron microscopy

Isolated thymocytes were fixed overnight with 2.5% glutaraldehyde in 0.1 M cacodylate buffer. Postfixation was carried out for 1 h at room temperature with a buffered 1% osmium tetroxide solution reduced with 1.5% potassium ferrocyanide. Samples were stained en bloc with 2.5% uranyl acetate. Cells were then rinsed and dehydrated using

gradually increasing concentrations of acetone to 100%. Infiltration of Spurr's epoxy resin and acetone was carried out over several days to 100% resin and cured 48 h in a 60 °C oven. Sections of 90 nm thickness were cut using an Ultracut E ultramicrotome (Reichert–Jung). Grids were then counterstained with 5% uranyl acetate for 2 min and Reynold's lead citrate for 2 min. Samples were imaged using a JEOL 1230 transmission electron microscope at 120 kV. To perform quantitative morphometry, 100 random images of both SOD2<sup>L/L</sup> and SOD2<sup>-/-</sup> thymocytes were chosen and blindly analyzed using ImageJ (National Institutes of Health) for the following parameters: cellular area, nuclear area, cytoplasmic area, number of mitochondria, mitochondrial perimeter, mitochondrial area, and mitochondrial density.

### Flow cytometry

T-cell-specific marker analysis for development or post-influenza infection was performed as previously described [50]. After isolation of fresh cell preparations, cells were suspended in staining buffer (HBSS supplemented with 5% bovine calf serum and 0.1% NaN<sub>3</sub>) and incubated with conjugated monoclonal antibodies in the presence of normal rat serum (to limit nonspecific antibody binding). After incubation and washing, the cells were suspended in fixative (1% formaldehyde in 1.25× PBS). Stained cells were run on a FACSVantage SE flow cytometer (Becton–Dickinson, Mountain View, CA, USA) with a minimum of 30,000 events collected per sample. Antibodies were semipurified from HB101 serum-free supernatants by 50% ammonium sulfate precipitation and conjugated to specific fluorescent dye by using standard procedures.

### Apoptosis and cell cycle

For apoptosis, the Annexin V–FITC Apoptosis Detection Kit (Becton–Dickinson) was used to assess annexin V-positive cells. Briefly, fresh cell preparations were incubated with 1× annexin binding buffer and annexin V–FITC (2.5 μg/ml)-conjugated primary antibody for 15 min on ice. After incubation, propidium iodide (PI; 10 μg/ml) was added to the suspension and the cells were analyzed by flow cytometry using an LSR flow cytometer. For cell cycle, analysis was adapted from a previously described report [51]. One million cells were centrifuged and suspended in 0.5 ml of Krishan reagent (0.1% Na citrate, 0.03% NP-40, 0.05 mg/ml PI, 0.02 mg/ml RNase A) before analysis. Analysis was performed by examining propidium iodide-stained nuclei on an LSR flow cytometer.

### Influenza and rescue

Mice (weighing approximately 20–25 g) were infected with 1600 TCID<sub>50</sub> of mouse-adapted A/PR/8/34 influenza virus A H1N1 by intranasal administration. For morbidity/mortality experiments, the mice were observed and weighed daily for 14 days. For pulmonary CD8<sup>+</sup> T cell analysis, mice were sacrificed at day 8 postinfection and T cells isolated from lung tissue. IAV PA224 (H2D(b)/SSLENFRAYV) and NP366 (H2D(b)/ASNENMETM) tetramers were obtained from the National Institute of Allergy and Infectious Disease MHC Tetramer Core Facility (Atlanta, GA, USA). For rescue experiments, Tempol was obtained from Sigma–Aldrich Co. Mito-CTPO was graciously donated by Dr. Balaraman Kalyanaraman (Medical College of Wisconsin). Both Tempol and Mito-CTPO were dissolved in ethanol vehicle and administered at 25 or 250 nM, respectively. Water bottles were supplemented with sucrose (4 g/100 ml) to offset the taste of the antioxidants. Mice were treated from the time of weaning until the date of experimentation.

### Statistics

Data are expressed as means and standard deviation. All experiments were performed on at least three mice. For most experiments,

comparisons between groups were analyzed by the unpaired two-tailed Student *t* test. For Kaplan–Meier analysis, log-rank analysis was performed. A *p* value of less than 0.01 was considered significant.

**Results**

*The conditional loss of SOD2 increases superoxide-specific oxidative stress in T cells*

Because of the lack of a sufficient model to study ROS stress on in vivo development of the mammalian adaptive immune system, we reasoned that the creation of a T-cell-specific SOD2 knockout mouse would serve as an optimal platform to study the effects of mitochondrial superoxide on immune system development and function. Floxed SOD2 mice were bred with mice expressing Cre recombinase under the control of the proximal promoter of Lck to the F2 generation to create homozygous T cell SOD2 knockouts. PCR analysis of tail sample DNA was used to confirm the proper genotype of animals used for studies (Supplemental Figs. 1A and B). After this, thymocytes were removed from animals to confirm the recombination of SOD2 in a tissue-specific manner. Genomic DNA extracted from T cells showed the specific excision product in SOD2<sup>-/-</sup> thymocytes, with no apparent Cre-recombination events in SOD2<sup>L/L</sup> animals (Fig. 1A). Furthermore, SOD2-specific mRNA levels were significantly decreased in knockout animals compared to control animals (Fig. 1B). T-cell-specific SOD2<sup>-/-</sup> mice were found to have minimal SOD2 protein and activity in thymus-derived T cells (Figs. 1C and D), whereas no significant decreases were noted in any off-target tissues (e.g., heart, liver, brain, pancreas, or muscle) in either SOD2<sup>-/-</sup> or SOD2<sup>L/L</sup> mice (data not shown). At every level of analysis, a small amount of residual SOD2 was detectable, suggesting the Cre recombination may have been incompletely penetrant or, alternatively, that our thymocyte preparations may contain non-Lck-expressing cells (i.e.,  $\gamma\delta$  T cells, immature T cell populations, or contaminating stromal cells) and thus do not possess Cre

recombinase. In either case, taken together, these data support the T cell specificity and efficiency of the model of SOD2 knockout.

To confirm that SOD2<sup>-/-</sup> mice did in fact harbor increased oxidative stress compared to their SOD2<sup>L/L</sup> littermates, we performed DHE stain flow cytometry as a relative measure of superoxide content within the T cell populations of these animals. It was observed that SOD2<sup>-/-</sup> mice demonstrated significantly increased steady-state levels of superoxide compared to control SOD2<sup>L/L</sup> mice (Fig. 2A). Importantly, no change was noted in nonspecific DHE oxidation or in the oxidation of a peroxide-sensitive probe, DCFH-DA (Fig. 2B). We confirmed and extended these findings in two separate enzyme activity assays that are highly specific to disruption by superoxide (aconitase and succinate dehydrogenase), as both were shown to be significantly decreased within the SOD2<sup>-/-</sup> T cells with no significant change in protein levels (Figs. 2C and D). It was previously shown that reactive nitrogen species (RNS) may also inactivate these enzymes [52], but probing cellular proteins for damage by RNS showed nondetectable levels of nitrotyrosine (data not shown). Overall, it appeared that the conditional loss of SOD2 caused a specific and significant increase in steady-state levels of superoxide within the T cell population of SOD2<sup>-/-</sup> mice; therefore these mice should serve as an effective model system for studying the effects of excess mitochondrial superoxide on the development and function of the mammalian T cell adaptive immune system.

*Increased mitochondrial superoxide levels perturb the normal development of murine T cells*

To understand the consequences of increased steady-state levels of mitochondrial superoxide during T cell growth and selection,

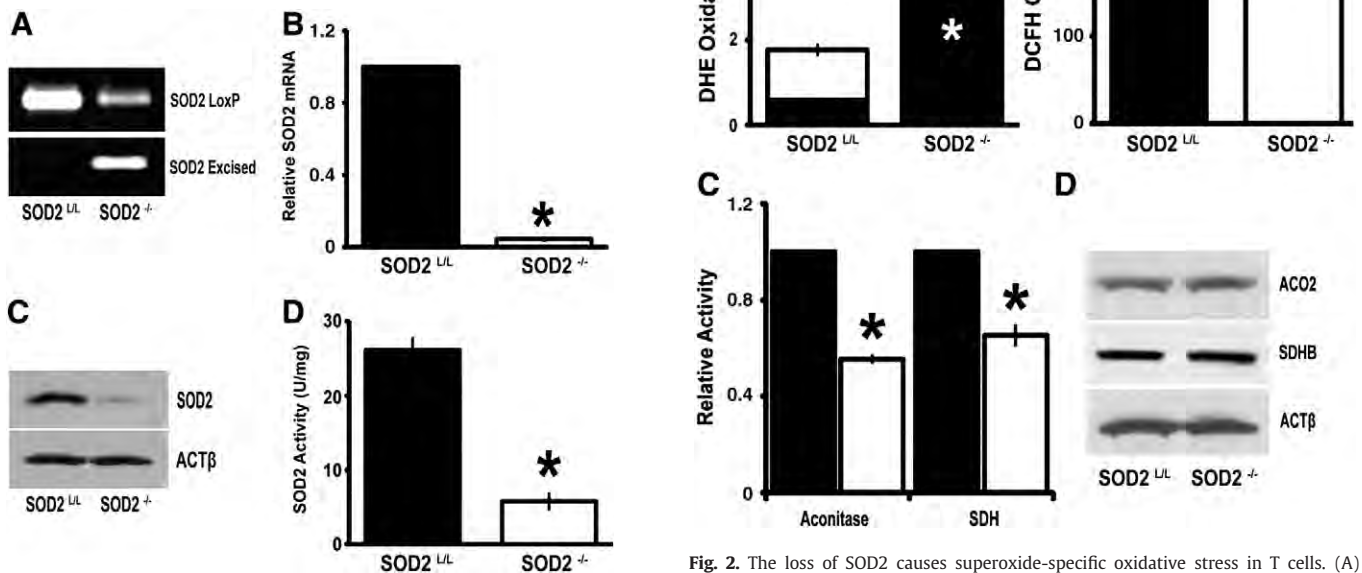


**Fig. 1.** SOD2 is conditionally and effectively removed from T cells. (A) Conventional PCR analysis of floxed or excised SOD2 products from genomic DNA extracted from 6-week-old SOD2<sup>L/L</sup> or SOD2<sup>-/-</sup> thymocytes. (B) Quantitative real-time RT-PCR analysis of SOD2 mRNA extracted from 6-week-old SOD2<sup>L/L</sup> or SOD2<sup>-/-</sup> thymocytes. Results are shown as normalized to SOD2<sup>L/L</sup>. (C) Comparison of SOD2 protein in 6-week-old SOD2<sup>L/L</sup> or SOD2<sup>-/-</sup> thymocytes.  $\beta$ -Actin (ACT $\beta$ ) is shown as a control for loading and transfer. (D) Activity assay performed on protein extracted from 6-week-old SOD2<sup>L/L</sup> or SOD2<sup>-/-</sup> thymocytes. At least three mice per experiment were analyzed; data are shown as means and SD. \**p* < 0.01 by Student's *t* test versus SOD2<sup>L/L</sup>.

**Fig. 2.** The loss of SOD2 causes superoxide-specific oxidative stress in T cells. (A) Quantification of total (entire bar) and superoxide-specific (black section of bar) DHE staining in 6-week-old thymocytes. (B) The peroxide-sensitive probe DCFH-DA demonstrated no significant change between SOD2<sup>L/L</sup> and SOD2<sup>-/-</sup> animals. (C) Quantification of total cellular aconitase and succinate dehydrogenase (SDH) activity in 6-week-old thymocytes. Black bars indicate SOD2<sup>L/L</sup> and open bars indicate SOD2<sup>-/-</sup>. (D) Western blots of the iron-sulfur-containing proteins aconitase 2 (ACO2) and succinate dehydrogenase B (SDHB) demonstrated no significant change in protein levels. For Western blots,  $\beta$ -actin (ACT $\beta$ ) is displayed as a control for loading and transfer. At least three mice per experiment were analyzed; data are shown as means and SD. \**p* < 0.01 by Student's *t* test versus SOD2<sup>L/L</sup>.

quantitative morphometry was performed on transmission electron microscopy (TEM) images of developing thymocytes (Fig. 3A). It was observed that cellular cross-sectional area was significantly increased within  $SOD2^{-/-}$  T cells, but no change was noted in nuclear area or mitochondrial size (Fig. 3B; Supplemental Figs. 2A and B). Conversely,  $SOD2^{-/-}$  thymocytes demonstrated an approximate doubling of the number of mitochondria per cell, but these mitochondria were less electron dense (Fig. 3B), suggesting dysfunctional or degrading organelles, as has been observed previously in oxidatively stressed systems [53]. These three mitochondrial parameters, decreased electron density, increased number per cell, and altered metabolism (Fig. 2C), all further support that the mitochondria within  $SOD2^{-/-}$  T cells are defective.

To expand upon these observations, the role of mitochondrial autophagy was explored. It was shown that autophagy was in fact increased in the  $SOD2^{-/-}$  T cells as shown by increases in autophagic vesicles and the cleaved form of LC-3 protein (Figs. 3C and D). Overall, the loss of SOD2 seems to have profound effects upon T cell ultrastructure as well as metabolic function.

In addition to the morphological changes, decreases in thymocyte numbers as well as peripheral T cells were noted (Fig. 4A). When total thymocytes were quantified at various ages throughout the mouse immune system development, an approximately twofold decrease was noted in  $SOD2^{-/-}$  mice. In contrast to this, mice harboring a SOD2 knockout from an earlier stage in development (i.e., Vav-iCre-mediated recombination) demonstrated no significant

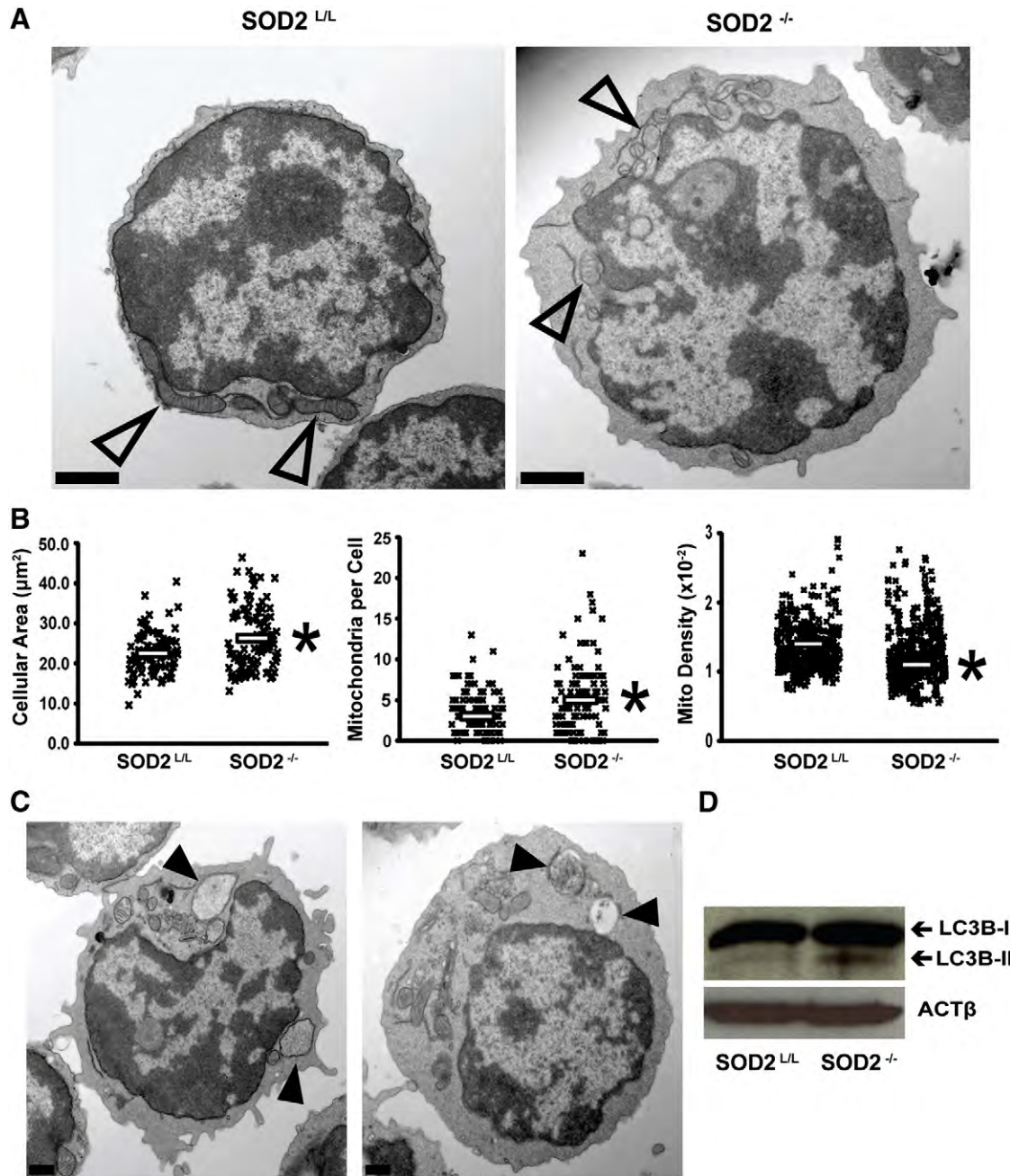


**Fig. 3.** Subcellular and mitochondrial alterations are consequences of T-cell-specific loss of SOD2. (A) Representative TEM images of  $SOD2^{L/L}$  (left) and  $SOD2^{-/-}$  (right) 6-week-old thymocytes. Open arrowheads indicate mitochondria. (B) Quantitative morphometry of thymocyte cellular area (left), mitochondrial number (center), and mitochondrial density (right). Each "X" represents one data analysis point; open bars represent means. (C) Representative TEM images of two  $SOD2^{-/-}$  6-week-old thymocytes. Solid arrowheads indicate apparent autophagic vesicles commonly seen in knockout animal thymocytes. (D) Western blot analysis comparing the increase in cleavage products (i.e., LC3B-II) of the autophagic marker LC3.  $\beta$ -Actin (ACT $\beta$ ) is shown as a control for loading and transfer. At least three mice per experiment were analyzed. \* $p < 0.01$  by Student's *t* test versus  $SOD2^{L/L}$ .

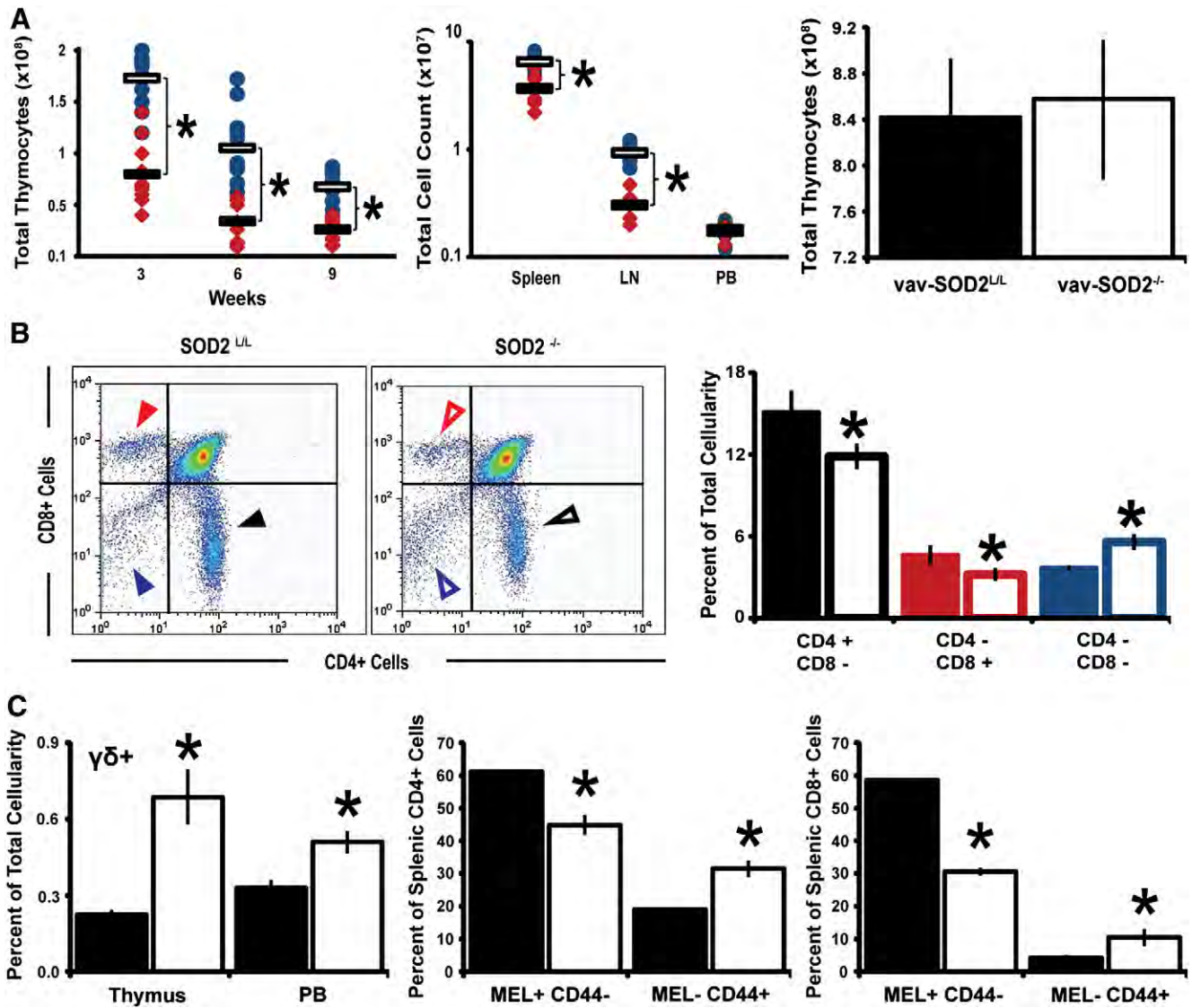


**Fig. 4.** Significant T cell developmental aberrations are observed in SOD2<sup>-/-</sup> animals. (A) Left: total thymic cellularity counts at various ages of T cell development for SOD2<sup>L/L</sup> (blue circles) and SOD2<sup>-/-</sup> (red diamonds) animals. Open bars show SOD2<sup>L/L</sup> averages, and solid bars show SOD2<sup>-/-</sup> averages. Middle: total cell counts for three peripheral lymphoid organs at 6 weeks of age. Right: total thymic cellularity counts for 6-week-old mice that were created using the Vav-iCre promoter. No significant change in thymic numbers is noted when knocking out SOD2 at a different stage in T cell development. (B) Left: representative flow scatter diagrams of SOD2<sup>L/L</sup> and SOD2<sup>-/-</sup> 6-week-old thymocytes for the developmental markers CD4 and CD8. Right: quantification of CD4<sup>+</sup> and CD8<sup>+</sup> 6-week-old thymocytes. Colored arrowheads (left) correlate to respective colored quantification (right); solid bars and arrowheads indicate SOD2<sup>L/L</sup> and open bars and arrowheads indicate SOD2<sup>-/-</sup>. (C) Quantification of flow cytometric analysis of  $\gamma\delta^+$  T cells (left), as well as for markers indicative of T cell activation, MEL14 and CD44, on splenic CD4<sup>+</sup> cells (middle) and CD8<sup>+</sup> cells (right). In all graphs, solid bars indicate SOD2<sup>L/L</sup> and open bars indicate SOD2<sup>-/-</sup>. At least three mice per experiment were analyzed; data are shown as means and SD. \* $p < 0.01$  by Student's *t* test versus SOD2<sup>L/L</sup>.

decrease in thymic cellularity (Fig. 4A, Supplemental Fig. 3A). This finding suggests that various stages in T cell development may be differentially sensitive to the presence of excess superoxide. Moreover, in contrast to the multiorgan failure noted in the aforementioned constitutive SOD2 knockout mouse [40], our preliminary studies have revealed no overt phenotype in unstressed animals harboring either liver-specific or mammary-specific knockouts of SOD2 (Supplemental Figs. 3A, B, and C). Taken together, the identification of a cellular defect in the T cell population due to the loss of SOD2 at a later (Lck-Cre-mediated) rather than an earlier (Vav-iCre-mediated) stage of development suggests that superoxide-mediated effects are tissue and time dependent and not a systemic non-specific phenomenon. Furthermore, the decrease in thymic cellularity of the Lck-Cre SOD2<sup>-/-</sup> mice was exacerbated by the fact that SOD2<sup>-/-</sup> mice also displayed reduced percentages of mature CD4<sup>+</sup> and CD8<sup>+</sup> thymocytes (Fig. 4B), a trend that was also observed in peripheral lymphoid organs as well (Supplemental Fig. 4B). In

contrast, the most immature T cell populations in the thymus (i.e., CD4<sup>-</sup>, CD8<sup>-</sup>),  $\gamma\delta$  T cells, as well as nonlymphocyte populations, were shown to be static or increased within SOD2<sup>-/-</sup> mice (Figs. 4B and C, Supplemental Fig. 4A). This is most likely attributable to the fact that none of these populations activates the Lck promoter and thus they do not express the exogenous Cre recombinase. Conversely, these populations may be exhibiting compensatory up-regulation due to the decrease in mature  $\alpha\beta$  T cells, a phenomenon that has been described in other models of T cell deficiencies [42,54]. Interestingly, while examining peripheral T cells, we observed that SOD2<sup>-/-</sup> lymphocytes expressed a greater proportion of MEL14<sup>-</sup>/CD44<sup>+</sup> cells, suggesting a more activated state among otherwise naïve T cells (Fig. 4C). This finding was further supported by microarray analysis that demonstrated up-regulation of numerous genes involved in T cell activation in the thymocytes of T cell SOD2<sup>-/-</sup> mice (Supplemental Figs. 5A and B), and a similar effect on gene regulation by mitochondrial superoxide has been recently reported [55]. An alternative hypothesis to

explain this apparently activated T cell phenotype could be the well-described phenomenon known as homeostatic expansion, a compensatory mechanism to replenish the global loss of T cells throughout the SOD2<sup>-/-</sup> mouse [56]. Taken together, these data suggest that increased mitochondrial-derived superoxide alters intracellular signaling within the developing thymocytes and may inappropriately mimic the activating conditions of an infection, thus inhibiting proper T cell function during true infection.

#### The decrease in SOD2<sup>-/-</sup> T cell numbers is due to increased apoptosis

During T cell development apoptosis is the major selective mechanism for lymphocyte death [57]. With the understanding that apoptosis may be initiated through cytochrome *c* release from damaged mitochondria or through the non-caspase-mediated p53 pathway [58], we postulated that increased apoptosis due to dysfunctional mitochondria may be the mechanism for decreased thymocytes in the SOD2<sup>-/-</sup> mice. When flow cytometry for annexin V/propidium iodide was performed, a twofold increase in the apoptotic fraction of thymocytes was found in the SOD2<sup>-/-</sup> mice (Fig. 5A). In addition, an approximate twofold increase in thymocyte sensitivity to oxygen toxicity *in vitro* as well as increased immunoreactive p53 was also noted, further suggesting increased susceptibility of SOD2<sup>-/-</sup> thymocytes to death by apoptosis (Supplemental Figs. 6B and C). In addition, propidium iodide cell cycle analysis demonstrated a greater cycling population

in SOD2<sup>-/-</sup> mice, which supports a role for compensatory proliferation in more primitive CD3<sup>-</sup>/CD4<sup>-</sup>/CD8<sup>-</sup> cells as previously discussed (Supplemental Fig. 6A). When mice were treated with small-molecule superoxide scavengers (i.e., Tempol [59] or Mito-CTPO [60]) added to the water supply from the time of weaning, the antioxidant supplementation led not only to the complete rescue of the SOD2<sup>-/-</sup> phenotype, but also to increased thymocyte numbers in control SOD2<sup>L/L</sup> animals by approximately twofold, while decreasing their apoptotic fraction by 50% (Fig. 5B). There was a strong correlation between apoptotic fractions and total cell counts, suggesting that apoptosis is the primary mechanism for increased T cell death in SOD2<sup>-/-</sup> animals (Fig. 5B). These data suggest a tight relationship between the regulation of steady-state mitochondrial superoxide levels within the normal developing thymus and immune system aberrations.

#### Mitochondrial superoxide mediates susceptibility to influenza A H1N1

The lack of proper T cell development observed in the SOD2<sup>-/-</sup> mice strongly suggested an immunocompromised state. To test this hypothesis, mice were challenged with a sublethal dose of IAV H1N1, a pathogen that causes a T-cell-mediated immune response, and their ability to mount an immune response was observed. Surprisingly, 100% of SOD2<sup>-/-</sup> animals succumbed to the infection and died, whereas only a small percentage of SOD2<sup>L/L</sup> animals exhibited mortality, and furthermore, SOD2<sup>-/-</sup> mice demonstrated increased

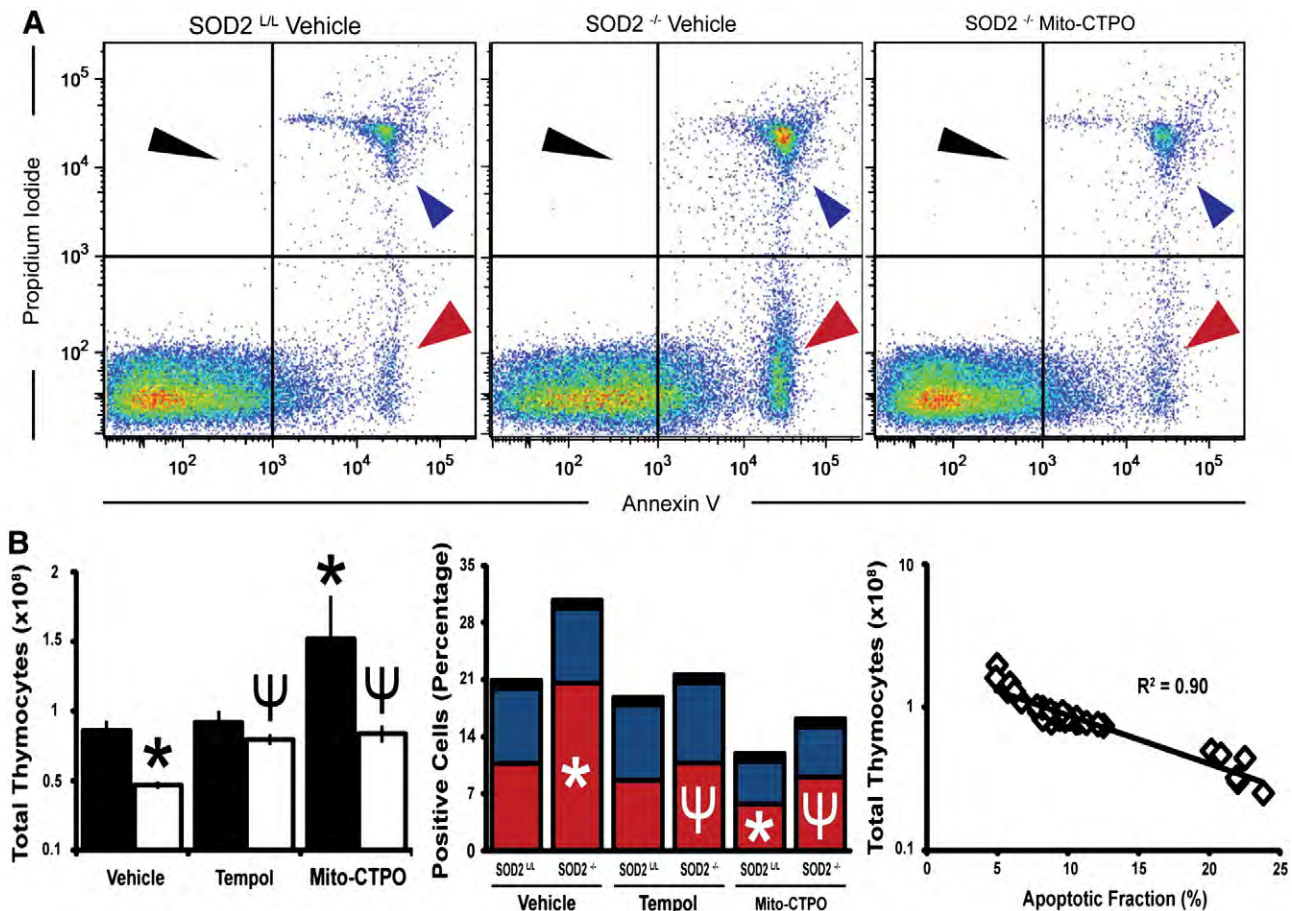


**Fig. 5.** Apoptosis explains the decrease in SOD2<sup>-/-</sup> thymocytes, which may be rescued by superoxide scavenger supplementation. (A) Representative annexin V and propidium iodide flow scatter diagrams of 6-week-old thymocytes from vehicle-treated SOD2<sup>L/L</sup> (left), vehicle-treated SOD2<sup>-/-</sup> (middle), and Mito-CTPO-treated SOD2<sup>-/-</sup> (right) mice. (B) Left: total thymic cellularity with and without pharmaceutical antioxidant supplementation. Middle: quantification of annexin V positive and propidium iodide negative thymocytes with and without pharmaceutical antioxidant supplementation. The colors are coordinated to the arrowheads in (A). Right: regression analysis of total thymic cellularity versus apoptotic fraction. At least three mice per experiment were analyzed; data are shown as means and SD. \**p*<0.01 by Student's *t* test versus vehicle-treated SOD2<sup>L/L</sup>. Ψ*p*<0.01 by Student's *t* test versus vehicle-treated SOD2<sup>-/-</sup>.

morbidity (i.e., weight loss) with no recovery compared to SOD2<sup>L/L</sup> mice (Fig. 6A). Moreover, treatment of SOD2<sup>-/-</sup> animals with the small-molecule superoxide scavenger Tempol (Supplemental Fig. 7) or Mito-CTPO (Fig. 6A) decreased this weight loss and rescued their ability to survive the influenza infection with delayed or no mortality noted. When examining immunological parameters of the infection, we once again found that SOD2<sup>-/-</sup> mice manifest their immune defect with decreases in not only total T cells, but also IAV-specific CD8<sup>+</sup> IAV-peptide-MHC-tetramer<sup>+</sup> cells, interferon- $\gamma$  (IFN- $\gamma$ )<sup>+</sup> cells, tumor necrosis factor  $\alpha$  (TNF- $\alpha$ )<sup>+</sup> cells, and dual-expressing IFN- $\gamma$ <sup>+</sup> TNF- $\alpha$ <sup>+</sup> cells (Fig. 6B; Supplemental Fig. 8A). Interestingly, of the SOD2<sup>-/-</sup> T cells that were present at the site of infection the quantity of IFN- $\gamma$  expression per cell was no less than in control SOD2<sup>L/L</sup> T cells, and TNF- $\alpha$  expression actually increased within SOD2<sup>-/-</sup> T-cells (Supplemental Fig. 8B). These findings are consistent with other studies of immunodeficient states and sepsis in which T cells compensate by overproducing proinflammatory markers in what is known as a “cytokine storm” [61] and may in part explain the apparently activated state of the naïve T cells in the SOD2<sup>-/-</sup> mice. Overall, alterations in mitochondrial superoxide steady-state levels seem to significantly affect the outcomes associated the mammalian adaptive response to viral infection.

**Discussion**

The current findings suggest an excess of mitochondrial superoxide at the stage of Lck activation of development tilts the intracellular redox potential toward apoptosis, resulting in the decreased thymic

cellularity observed. A relative increase in the normal steady-state levels of superoxide had severe consequences on the immunocompetence of the mammalian adaptive immune system. This novel finding complements the well-established role of ROS in the innate immune system and adds yet another effect of superoxide and its derived reactive oxygen intermediates on normal tissue growth and development. However, further studies are required to examine specific signaling pathways that are affected by increased mitochondrial superoxide. It would be predicted that redox-sensitive signaling cascades such as NF- $\kappa$ B [17], AP-1 [15], or JAK/STAT [18] may be affected and, as such, may in part in explaining the pseudo-activated state and microarray results observed in this study. Furthermore, the role of posttranslational modifications on proteins such as the hypoxia-inducible factor could also provide valuable information on how ROS regulate cellular signaling [62]. Moreover, how ROS affect peripheral lymphocyte mitosis, proliferation, and expansion in antigen-unchallenged and -challenged mice also warrants further examination. It may also be beneficial to understand the role of compartmentalization of superoxide (e.g., cytoplasmic, extracellular), and as such these studies should be followed by similar investigations using SOD1 [63] or SOD3 [64] conditional knockout animals. Because both SOD1 and SOD3 constitutive knockout animals are viable and have no gross pathologic phenotype compared to the constitutive SOD2 knockout mouse [31,39,40,65], it would be postulated that superoxide compartmentalization may explain this phenomenon at least in part. We observed that elevated mitochondrial superoxide levels had severe effects on T cell development, but it may be postulated that elevated superoxide in different cellular and tissue

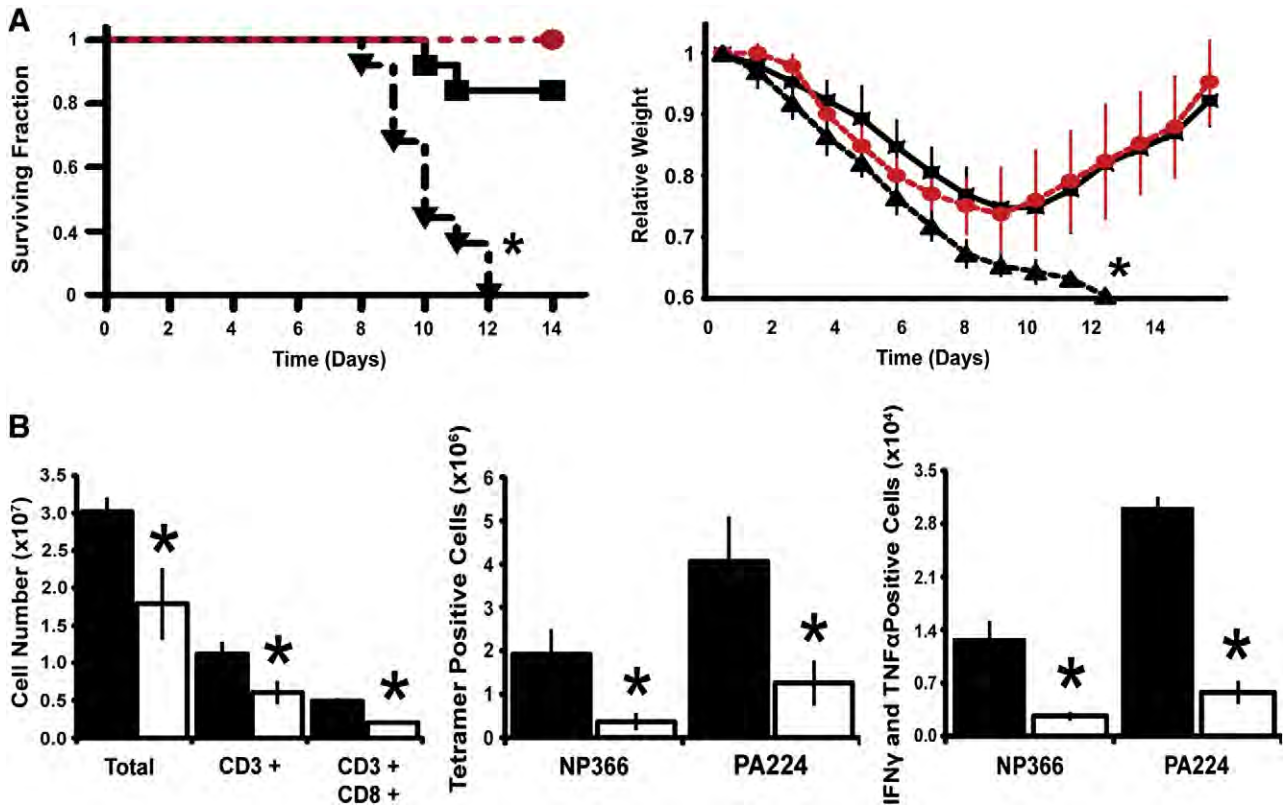


**Fig. 6.** SOD2<sup>-/-</sup> mice are immunologically susceptible to influenza virus, but may be rescued by superoxide-scavenging pharmaceuticals. (A) Left: Kaplan–Meier analysis of mice succumbing to IAV H1N1 infection during a 2-week period after viral administration with and without Mito-CTPO administration. Right: relative weight loss of mice over a two-week period after infection with IAV with and without Mito-CTPO supplementation. Squares, vehicle-treated SOD2<sup>L/L</sup>; triangles, vehicle-treated SOD2<sup>-/-</sup>; circles, Mito-CTPO-treated SOD2<sup>-/-</sup>. (B) Left: total lymphocyte counts harvested from lungs of both SOD2<sup>L/L</sup> and SOD2<sup>-/-</sup> animals 8 days post-influenza virus infection. Also, flow cytometric analysis of CD8<sup>+</sup> influenza-specific NP366 and PA224 MHC-tetramer-positive cells (middle) and analysis of NP366- and PA224-specific IFN- $\gamma$ <sup>+</sup>/TNF- $\alpha$ <sup>+</sup> (right) CD8<sup>+</sup> T cells isolated from lungs 8 days post-IAV H1N1 infection. At least six mice per experiment were analyzed; data are shown as means and SD. For weights and bar graphs, \**p*<0.01 by Student’s *t* test versus SOD2<sup>L/L</sup>. For mortality, \**p*<0.01 by log-rank analysis versus SOD2<sup>L/L</sup>.

compartments may lead to a spectrum of developmental, functional, or disease (e.g., cancer) predispositions. Last, we have examined mitochondrial superoxide and the consequences of its excess on the development of the T cell adaptive immune system. An in-depth analysis of other reactive oxygen species (e.g., hydrogen peroxide, peroxynitrite, hydroxyl radical) may prove highly informative to further understand the part each plays in the development and function of organ systems. These data could serve as a platform for targeting specific immunodeficiencies that are currently not well understood and may be due to alterations in redox status and tailoring antioxidant therapies accordingly.

In this study, it was demonstrated that the loss of immunocompetence in a SOD2<sup>-/-</sup> background could be rescued using a mitochondria-targeted superoxide scavenger, an example of the aforementioned tailoring of specific therapies to immunodeficiencies. Serendipitously, it was shown that SOD2<sup>L/L</sup> mice with fully developed and functional adaptive immune systems also responded to the pharmaceutical intervention. These mice were shown to have significantly increased numbers of thymocytes compared to untreated control animals, and this seemed to be due to a decreased apoptotic fraction. At first glance, it seems that this increase in T cells could potentially be a boost to immune system prowess, but SOD2<sup>L/L</sup> mice treated with superoxide scavengers showed no significant increase/decrease in the ability to recover from influenza A, H1N1, infection (data not shown). This finding is most probably attributable to the hypothesis that the increase in T cells is due to an inhibition of proper apoptotic death of cells destined to die in the thymus (i.e., nonfunctional cells, cells that are self-recognizing, etc.) as opposed to the expansion of pathogen-specific immune cells. Although in the short term this had no observable consequence, it is speculated that the preservation of cells predestined for death could lead to the potential for autoimmunity. Additional studies will be needed to confirm this potential role of superoxide in the development of autoimmune diseases in both mouse and human. In this study, equal numbers of male and female mice were used for all assays, but anecdotally it was observed in many cases that females demonstrated more pronounced outcomes due to the effects of altering steady-state superoxide levels. With the understanding that females are more prone to autoimmune diseases, as well as the recent observation of different antioxidant capacities in females and males [66], this preliminary observation may warrant further examination of this phenomenon in similar models of adaptive immune system antioxidant alterations.

In conclusion, we have used a previously undescribed model of T-cell-specific superoxide scavenging deficiency to examine the development of the adaptive branch of the mammalian immune system and found that excess mitochondrial superoxide late in T cell development is detrimental to normal T cell maturation. In contrast, early developmental loss of SOD2 activity displayed no gross alteration in thymic cellularity, indicating the importance of the temporal nature of the loss of SOD2 function on thymic developmental processes. In addition, we have shown that the loss of SOD2 does not exert a similar damaging effect in development or maturation of other organs, including liver and mammary glands, supporting previous findings by others using SOD2 floxed models [37,67]. At this time the nature of the differences in cell-type specificity and developmental timing of superoxide toxicity are poorly understood, but our findings warrant further investigation into possible mechanisms mediating these differential sensitivities. Using the appropriate Cre-recombinase mouse, this model could be expanded to examining other elements of the immune system (e.g., B cells [68], neutrophils [69], macrophages [69]), different time points in development [41,42,70], or other organ systems altogether [53,71,72]. In addition, because of the simplicity of the breeding scheme the floxed SOD2 mouse may be applied in combination with other protein deletions or additions (e.g., p53 null [73], Myc overexpression [74,75]) to examine

the effect of superoxide oxidative stress in alternative immune model systems. Overall, this new model and these observations serve as an initial step in understanding the role of ROS in development and function of mammalian organ systems.

## Acknowledgments

We thank The University of Iowa Animal Pathology, Central Microscopy, and Flow Cytometry Facilities, especially David Meyerholz and Kathy Walters, for their help in tissue preparation and analysis. Microarray data were generated by the Genomics Core at the Arizona Cancer Center, supported by the Southwest Environmental Health Sciences Center. In addition, we are grateful to George Watts, Jose Munoz-Rodriguez, David Motto, Stephen Sangster, Joshua Madsen, Anna Johns, Melissa Teoh-Fitzgerald, Sean Martin, and C. Michael Knudson for their technical help or supplies. Last, we thank Adam Dupuy, Curt Sigmund, Balaraman Kalyanaraman, Joy Joseph, and Takamune Takahashi for their generous donations. This work was supported by the following grants: NIH RO1 CA073612, DOD PC073831, NIAAA AA019438, NIAAA AA019437, NIAID AI071085, NIH P30 CA086862, DOE-DE-SC0000830.

## Appendix A. Supplementary material

Supplementary data to this article can be found online at doi:10.1016/j.freeradbiomed.2010.11.025.

## References

- [1] McCord, J. M.; Fridovich, I. The biology and pathology of oxygen radicals. *Ann. Intern. Med.* **89**:122–127; 1978.
- [2] Cerutti, P. A. Prooxidant states and tumor promotion. *Science* **227**:375–381; 1985.
- [3] Fridovich, I. Oxygen toxicity: a radical explanation. *J. Exp. Biol.* **201**:1203–1209; 1998.
- [4] Leibovitz, B. E.; Siegel, B. V. Aspects of free radical reactions in biological systems: aging. *J. Gerontol.* **35**:45–56; 1980.
- [5] Kaneto, H.; Katakami, N.; Matsuhisa, M.; Matsuoka, T. A. Role of reactive oxygen species in the progression of type 2 diabetes and atherosclerosis. *Mediat. Inflamm.* **2010**:453892; 2010.
- [6] Miao, L.; St Clair, D. K. Regulation of superoxide dismutase genes: implications in disease. *Free Radic. Biol. Med.* **47**:344–356; 2009.
- [7] Nunomura, A.; Hofer, T.; Moreira, P. I.; Castellani, R. J.; Smith, M. A.; Perry, G. RNA oxidation in Alzheimer disease and related neurodegenerative disorders. *Acta Neuropathol.* **118**:151–166; 2009.
- [8] Oberley, L. W.; Buettner, G. R. Role of superoxide dismutase in cancer: a review. *Cancer Res.* **39**:1141–1149; 1979.
- [9] Akaike, T.; Ando, M.; Oda, T.; Doi, T.; Ijiri, S.; Araki, S.; Maeda, H. Dependence on O<sub>2</sub><sup>-</sup> generation by xanthine oxidase of pathogenesis of influenza virus infection in mice. *J. Clin. Invest.* **85**:739–745; 1990.
- [10] Oda, T.; Akaike, T.; Hamamoto, T.; Suzuki, F.; Hirano, T.; Maeda, H. Oxygen radicals in influenza-induced pathogenesis and treatment with pyran polymer-conjugated SOD. *Science* **244**:974–976; 1989.
- [11] Geiler, J.; Michaelis, M.; Naczek, P.; Leutz, A.; Langer, K.; Doerr, H. W.; Cinatl Jr., J. N-acetyl-L-cysteine (NAC) inhibits virus replication and expression of pro-inflammatory molecules in A549 cells infected with highly pathogenic H5N1 influenza A virus. *Biochem. Pharmacol.* **79**:413–420; 2009.
- [12] Jariwalla, R. J.; Roomi, M. W.; Gangapurkar, B.; Kalinovsky, T.; Niedzwiecki, A.; Rath, M. Suppression of influenza A virus nuclear antigen production and neuraminidase activity by a nutrient mixture containing ascorbic acid, green tea extract and amino acids. *Biofactors* **31**:1–15; 2007.
- [13] Sidwell, R. W.; Huffman, J. H.; Bailey, K. W.; Wong, M. H.; Nimrod, A.; Panet, A. Inhibitory effects of recombinant manganese superoxide dismutase on influenza virus infections in mice. *Antimicrob. Agents Chemother.* **40**:2626–2631; 1996.
- [14] Suliman, H. B.; Ryan, L. K.; Bishop, L.; Folz, R. J. Prevention of influenza-induced lung injury in mice overexpressing extracellular superoxide dismutase. *Am. J. Physiol. Lung Cell. Mol. Physiol.* **280**:L69–L78; 2001.
- [15] Gius, D.; Botero, A.; Shah, S.; Curry, H. A. Intracellular oxidation/reduction status in the regulation of transcription factors NF-kappaB and AP-1. *Toxicol. Lett.* **106**:93–106; 1999.
- [16] Gius, D.; Spitz, D. R. Redox signaling in cancer biology. *Antioxid. Redox Signaling* **8**:1249–1252; 2006.
- [17] Schulze-Osthoff, K.; Los, M.; Baeuerle, P. A. Redox signalling by transcription factors NF-kappa B and AP-1 in lymphocytes. *Biochem. Pharmacol.* **50**:735–741; 1995.
- [18] Uckun, F. M.; Qazi, S.; Ma, H.; Tuel-Ahlgren, L.; Ozer, Z. STAT3 is a substrate of SYK tyrosine kinase in B-lineage leukemia/lymphoma cells exposed to oxidative stress. *Proc. Natl Acad. Sci. USA* **107**:2902–2907; 2010.

- [19] Allen, R. G.; Balin, A. K. Oxidative influence on development and differentiation: an overview of a free radical theory of development. *Free Radic. Biol. Med.* **6**:631–661; 1989.
- [20] Hitchler, M. J.; Domann, F. E. An epigenetic perspective on the free radical theory of development. *Free Radic. Biol. Med.* **43**:1023–1036; 2007.
- [21] Tauber, A. I.; Babior, B. M. Evidence for hydroxyl radical production by human neutrophils. *J. Clin. Invest.* **60**:374–379; 1977.
- [22] Lu, S. P.; Lin Feng, M. H.; Huang, H. L.; Huang, Y. C.; Tsou, W. I.; Lai, M. Z. Reactive oxygen species promote raft formation in T lymphocytes. *Free Radic. Biol. Med.* **42**:936–944; 2007.
- [23] Norell, H.; Martins da Palma, T.; Leshner, A.; Kaur, N.; Mehrotra, M.; Naga, O. S.; Spivey, N.; Olafimihan, S.; Chakraborty, N. G.; Voelkel-Johnson, C.; Nishimura, M. I.; Mukherji, B.; Mehrotra, S. Inhibition of superoxide generation upon T-cell receptor engagement rescues Mart-1(27-35)-reactive T cells from activation-induced cell death. *Cancer Res.* **69**:6282–6289; 2009.
- [24] Sklavos, M. M.; Tse, H. M.; Piganelli, J. D. Redox modulation inhibits CD8 T cell effector function. *Free Radic. Biol. Med.* **45**:1477–1486; 2008.
- [25] Niethammer, P.; Grabher, C.; Look, A. T.; Mitchison, T. J. A tissue-scale gradient of hydrogen peroxide mediates rapid wound detection in zebrafish. *Nature* **459**:996–999; 2009.
- [26] Owusu-Ansah, E.; Banerjee, U. Reactive oxygen species prime *Drosophila* haematopoietic progenitors for differentiation. *Nature* **461**:537–541; 2009.
- [27] Macho, A.; Hirsch, T.; Marzo, I.; Marchetti, P.; Dallaporta, B.; Susin, S. A.; Zamzami, N.; Kroemer, G. Glutathione depletion is an early and calcium elevation is a late event of thymocyte apoptosis. *J. Immunol.* **158**:4612–4619; 1997.
- [28] Choi, J.; Oh, S.; Lee, D.; Oh, H. J.; Park, J. Y.; Lee, S. B.; Lim, D. S. Mst1–FoxO signaling protects naive T lymphocytes from cellular oxidative stress in mice. *PLoS ONE* **4**:e8011; 2009.
- [29] Moulian, N.; Truffault, F.; Gaudry-Talarmin, Y. M.; Serraf, A.; Berrih-Aknin, S. In vivo and in vitro apoptosis of human thymocytes are associated with nitrotyrosine formation. *Blood* **97**:3521–3530; 2001.
- [30] Peled-Kamar, M.; Lotem, J.; Okon, E.; Sachs, L.; Groner, Y. Thymic abnormalities and enhanced apoptosis of thymocytes and bone marrow cells in transgenic mice overexpressing Cu/Zn-superoxide dismutase: implications for Down syndrome. *EMBO J.* **14**:4985–4993; 1995.
- [31] Carlsson, L. M.; Jonsson, J.; Edlund, T.; Marklund, S. L. Mice lacking extracellular superoxide dismutase are more sensitive to hyperoxia. *Proc. Natl Acad. Sci. USA* **92**:6264–6268; 1995.
- [32] Elchuri, S.; Oberley, T. D.; Qi, W.; Eisenstein, R. S.; Jackson Roberts, L.; Van Remmen, H.; Epstein, C. J.; Huang, T. T. CuZnSOD deficiency leads to persistent and widespread oxidative damage and hepatocarcinogenesis later in life. *Oncogene* **24**:367–380; 2005.
- [33] Ho, Y. S.; Gargano, M.; Cao, J.; Bronson, R. T.; Heimler, I.; Hutz, R. J. Reduced fertility in female mice lacking copper–zinc superoxide dismutase. *J. Biol. Chem.* **273**:7765–7769; 1998.
- [34] Ho, Y. S.; Magnenat, J. L.; Bronson, R. T.; Cao, J.; Gargano, M.; Sugawara, M.; Funk, C. D. Mice deficient in cellular glutathione peroxidase develop normally and show no increased sensitivity to hyperoxia. *J. Biol. Chem.* **272**:16644–16651; 1997.
- [35] Ho, Y. S.; Xiong, Y.; Ma, W.; Spector, A.; Ho, D. S. Mice lacking catalase develop normally but show differential sensitivity to oxidant tissue injury. *J. Biol. Chem.* **279**:32804–32812; 2004.
- [36] Sentman, M. L.; Granstrom, M.; Jakobson, H.; Reaume, A.; Basu, S.; Marklund, S. L. Phenotypes of mice lacking extracellular superoxide dismutase and copper- and zinc-containing superoxide dismutase. *J. Biol. Chem.* **281**:6904–6909; 2006.
- [37] Ikegami, T.; Suzuki, Y.; Shimizu, T.; Isono, K.; Koseki, H.; Shirasawa, T. Model mice for tissue-specific deletion of the manganese superoxide dismutase (MnSOD) gene. *Biochem. Biophys. Res. Commun.* **296**:729–736; 2002.
- [38] Fridovich, I. The biology of oxygen radicals. *Science* **201**:875–880; 1978.
- [39] Lebovitz, R. M.; Zhang, H.; Vogel, H.; Cartwright Jr., J.; Dionne, L.; Lu, N.; Huang, S.; Matzuk, M. M. Neurodegeneration, myocardial injury, and perinatal death in mitochondrial superoxide dismutase-deficient mice. *Proc. Natl Acad. Sci. USA* **93**:9782–9787; 1996.
- [40] Li, Y.; Huang, T. T.; Carlson, E. J.; Melov, S.; Ursell, P. C.; Olson, J. L.; Noble, L. J.; Yoshimura, M. P.; Berger, C.; Chan, P. H.; Wallace, D. C.; Epstein, C. J. Dilated cardiomyopathy and neonatal lethality in mutant mice lacking manganese superoxide dismutase. *Nat. Genet.* **11**:376–381; 1995.
- [41] de Boer, J.; Williams, A.; Skavdis, G.; Harker, N.; Coles, M.; Tolaini, M.; Norton, T.; Williams, K.; Roderick, K.; Potocnik, A. J.; Kioussis, D. Transgenic mice with hematopoietic and lymphoid specific expression of Cre. *Eur. J. Immunol.* **33**:314–325; 2003.
- [42] Lee, P. P.; Fitzpatrick, D. R.; Beard, C.; Jessup, H. K.; Lehar, S.; Makar, K. W.; Perez-Melgosa, M.; Sweetser, M. T.; Schlissel, M. S.; Nguyen, S.; Cherry, S. R.; Tsai, J. H.; Tucker, S. M.; Weaver, W. M.; Kelso, A.; Jaenisch, R.; Wilson, C. B. A critical role for Dnmt1 and DNA methylation in T cell development, function, and survival. *Immunity* **15**:763–774; 2001.
- [43] Postic, C.; Shiota, M.; Niswender, K. D.; Jetton, T. L.; Chen, Y.; Moates, J. M.; Shelton, K. D.; Lindner, J.; Cherrington, A. D.; Magnuson, M. A. Dual roles for glucokinase in glucose homeostasis as determined by liver and pancreatic beta cell-specific gene knock-outs using Cre recombinase. *J. Biol. Chem.* **274**:305–315; 1999.
- [44] Wagner, K. U.; Wall, R. J.; St-Onge, L.; Gruss, P.; Wynshaw-Boris, A.; Garrett, L.; Li, M.; Furth, P. A.; Hennighausen, L. Cre-mediated gene deletion in the mammary gland. *Nucleic Acids Res.* **25**:4323–4330; 1997.
- [45] Spitz, D. R.; Oberley, L. W. An assay for superoxide dismutase activity in mammalian tissue homogenates. *Anal. Biochem.* **179**:8–18; 1989.
- [46] Robinson, K. M.; Janes, M. S.; Pehar, M.; Monette, J. S.; Ross, M. F.; Hagen, T. M.; Murphy, M. P.; Beckman, J. S. Selective fluorescent imaging of superoxide in vivo using ethidium-based probes. *Proc. Natl Acad. Sci. USA* **103**:15038–15043; 2006.
- [47] Slane, B. G.; Aykin-Burns, N.; Smith, B. J.; Kalen, A. L.; Goswami, P. C.; Domann, F. E.; Spitz, D. R. Mutation of succinate dehydrogenase subunit C results in increased O<sub>2</sub><sup>-</sup>, oxidative stress, and genomic instability. *Cancer Res.* **66**:7615–7620; 2006.
- [48] Morton, R. L.; Ikle, D.; White, C. W. Loss of lung mitochondrial aconitase activity due to hyperoxia in bronchopulmonary dysplasia in primates. *Am. J. Physiol.* **274**:L127–L133; 1998.
- [49] Guzy, R. D.; Sharma, B.; Bell, E.; Chandel, N. S.; Schumacker, P. T. Loss of the SdhB, but not the SdhA, subunit of complex II triggers reactive oxygen species-dependent hypoxia-inducible factor activation and tumorigenesis. *Mol. Cell. Biol.* **28**:718–731; 2008.
- [50] Rijhsinghani, A. G.; Bhatia, S. K.; Tygrett, L. T.; Waldschmidt, T. J. Effect of pregnancy on thymic T cell development. *Am. J. Reprod. Immunol.* **35**:523–528; 1996.
- [51] Knudson, C. M.; Johnson, G. M.; Lin, Y.; Korsmeyer, S. J. Bax accelerates tumorigenesis in p53-deficient mice. *Cancer Res.* **61**:659–665; 2001.
- [52] Tortora, V.; Quijano, C.; Freeman, B.; Radi, R.; Castro, L. Mitochondrial aconitase reaction with nitric oxide, S-nitrosoglutathione, and peroxynitrite: mechanisms and relative contributions to aconitase inactivation. *Free Radic. Biol. Med.* **42**:1075–1088; 2007.
- [53] Misawa, H.; Nakata, K.; Matsuura, J.; Moriwaki, Y.; Kawashima, K.; Shimizu, T.; Shirasawa, T.; Takahashi, R. Conditional knockout of Mn superoxide dismutase in postnatal motor neurons reveals resistance to mitochondrial generated superoxide radicals. *Neurobiol. Dis.* **23**:169–177; 2006.
- [54] Molina, T. J.; Kishihara, K.; Siderovski, D. P.; van Ewijk, W.; Narendran, A.; Timms, E.; Wakeham, A.; Paige, C. J.; Hartmann, K. U.; Veillette, A., et al. Profound block in thymocyte development in mice lacking p56lck. *Nature* **357**:161–164; 1992.
- [55] Kaminski, M. M.; Sauer, S. W.; Klemke, C. D.; Suss, D.; Okun, J. G.; Krammer, P. H.; Gulow, K. Mitochondrial reactive oxygen species control T cell activation by regulating IL-2 and IL-4 expression: mechanism of ciprofloxacin-mediated immunosuppression. *J. Immunol.* **184**:4827–4841; 2010.
- [56] King, C.; Ilic, A.; Koelsch, K.; Sarvetnick, N. Homeostatic expansion of T cells during immune insufficiency generates autoimmunity. *Cell* **117**:265–277; 2004.
- [57] Williams, G. T. Role of apoptosis in the immune system. *Biochem. Cell Biol.* **72**:447–450; 1994.
- [58] Liu, J.; Cao, L.; Chen, J.; Song, S.; Lee, I. H.; Quijano, C.; Liu, H.; Keyvanfar, K.; Chen, H.; Cao, L. Y.; Ahn, B. H.; Kumar, N. G.; Rovira, I. I.; Xu, X. L.; van Lohuizen, M.; Motoyama, N.; Deng, C. X.; Finkel, T. Bmi1 regulates mitochondrial function and the DNA damage response pathway. *Nature* **459**:387–392; 2009.
- [59] Mitchell, J. B.; Xavier, S.; DeLuca, A. M.; Sowers, A. L.; Cook, J. A.; Krishna, M. C.; Hahn, S. M.; Russo, A. A low molecular weight antioxidant decreases weight and lowers tumor incidence. *Free Radic. Biol. Med.* **34**:93–102; 2003.
- [60] Dhanasekaran, A.; Kotamraju, S.; Karunakaran, C.; Kalivendi, S. V.; Thomas, S.; Joseph, J.; Kalyanaraman, B. Mitochondria superoxide dismutase mimetic inhibits peroxide-induced oxidative damage and apoptosis: role of mitochondrial superoxide. *Free Radic. Biol. Med.* **39**:567–583; 2005.
- [61] Wang, H.; Ma, S. The cytokine storm and factors determining the sequence and severity of organ dysfunction in multiple organ dysfunction syndrome. *Am. J. Emerg. Med.* **26**:711–715; 2008.
- [62] Kaewpila, S.; Venkataraman, S.; Buettner, G. R.; Oberley, L. W. Manganese superoxide dismutase modulates hypoxia-inducible factor-1 alpha induction via superoxide. *Cancer Res.* **68**:2781–2788; 2008.
- [63] Gong, Y. H.; Parsadanian, A. S.; Andreeva, A.; Snider, W. D.; Elliott, J. L. Restricted expression of G86R Cu/Zn superoxide dismutase in astrocytes results in astrocytosis but does not cause motoneuron degeneration. *J. Neurosci.* **20**:660–665; 2000.
- [64] Gongora, M. C.; Lob, H. E.; Landmesser, U.; Guzik, T. J.; Martin, W. D.; Ozumi, K.; Wall, S. M.; Wilson, D. S.; Murthy, N.; Gravanis, M.; Fukai, T.; Harrison, D. G. Loss of extracellular superoxide dismutase leads to acute lung damage in the presence of ambient air: a potential mechanism underlying adult respiratory distress syndrome. *Am. J. Pathol.* **173**:915–926; 2008.
- [65] Reaume, A. G.; Elliott, J. L.; Hoffman, E. K.; Kowall, N. W.; Ferrante, R. J.; Siwek, D. F.; Wilcox, H. M.; Flood, D. G.; Beal, M. F.; Brown Jr., R. H.; Scott, R. W.; Snider, W. D. Motor neurons in Cu/Zn superoxide dismutase-deficient mice develop normally but exhibit enhanced cell death after axonal injury. *Nat. Genet.* **13**:43–47; 1996.
- [66] Kim, A.; Joseph, S.; Khan, A.; Epstein, C. J.; Sobel, R.; Huang, T. T. Enhanced expression of mitochondrial superoxide dismutase leads to prolonged in vivo cell cycle progression and up-regulation of mitochondrial thioredoxin. *Free Radic. Biol. Med.* **48**:1501–1512; 2010.
- [67] Shimizu, T.; Nojiri, H.; Kawakami, S.; Uchiyama, S.; Shirasawa, T. Model mice for tissue-specific deletion of the manganese superoxide dismutase gene. *Geriatr. Gerontol. Int.* **10** (Suppl. 1):S70–S79; 2010.
- [68] Rickert, R. C.; Roes, J.; Rajewsky, K. B lymphocyte-specific, Cre-mediated mutagenesis in mice. *Nucleic Acids Res.* **25**:1317–1318; 1997.
- [69] Clausen, B. E.; Burkhardt, C.; Reith, W.; Renkawitz, R.; Forster, I. Conditional gene targeting in macrophages and granulocytes using LysMcre mice. *Transgenic Res.* **8**:265–277; 1999.
- [70] Maekawa, Y.; Minato, Y.; Ishifune, C.; Kurihara, T.; Kitamura, A.; Kojima, H.; Yagita, H.; Sakata-Yanagimoto, M.; Saito, T.; Taniuchi, I.; Chiba, S.; Sone, S.; Yasutomo, K. Notch2 integrates signaling by the transcription factors RBP-J and CREB1 to promote T cell cytotoxicity. *Nat. Immunol.* **9**:1140–1147; 2008.
- [71] Lenart, J.; Dombrowski, F.; Grolach, A.; Kietzmann, T. Deficiency of manganese superoxide dismutase in hepatocytes disrupts zoned gene expression in mouse liver. *Arch. Biochem. Biophys.* **462**:238–244; 2007.
- [72] Lustgarten, M.; Jang, Y.; Liu, Y.; Muller, F.; Qi, W.; Steinhilber, M.; Brooks, S.; Larkin, L. M.; Shimizu, T.; Shirasawa, T.; McManus, L.; Bhattacharya, A.; Richardson, A.; Van Remmen, H. Conditional knockout of MnSOD targeted to type IIB skeletal muscle fibers increases oxidative stress and is sufficient to alter aerobic exercise capacity. *Am. J. Physiol. Cell Physiol.* **297**:C1520–C1532; 2009.

- [73] Jonkers, J.; Meuwissen, R.; van der Gulden, H.; Peterse, H.; van der Valk, M.; Berns, A. Synergistic tumor suppressor activity of BRCA2 and p53 in a conditional mouse model for breast cancer. *Nat. Genet.* **29**:418–425; 2001.
- [74] Park, S. S.; Kim, J. S.; Tessarollo, L.; Owens, J. D.; Peng, L.; Han, S. S.; Tae Chung, S.; Torrey, T. A.; Cheung, W. C.; Polakiewicz, R. D.; McNeil, N.; Ried, T.; Mushinski, J. F.; Morse III, H. C.; Janz, S. Insertion of c-Myc into Igh induces B-cell and plasma-cell neoplasms in mice. *Cancer Res.* **65**:1306–1315; 2005.
- [75] Park, S. S.; Shaffer, A. L.; Kim, J. S.; duBois, W.; Potter, M.; Staudt, L. M.; Janz, S. Insertion of Myc into Igh accelerates peritoneal plasmacytomas in mice. *Cancer Res.* **65**:7644–7652; 2005.